# CHARACTERIZATION OF COMPRESSIVE DAMAGE MECHANISMS IN CERAMIC AND POLYMERIC MATRIX COMPOSITE MATERIALS

By

James Lankford, Jr.

TECHNICAL REPORT
ONR Contract No. N00014-92-C-0093
ONR Contract Authority NR 032-553
SwRI Project 06-5035

Prepared for

Office of Naval Research
Arlington, VA 22217

Prepared by

Southwest Research Institute
San Antonio, Texas

February 1995

SOUTHWEST RESEARCH INSTITUTE
SAN ANTONIO
DETROIT
HOUSTON
WASHINGTON, DC

UNCLASSIFIED

SECURITY CLASSIFICATION OF THIS PAGE

# REPORT DOCUMENTATION PAGE

*Form Approved*
*OMB No. 0704-0188*
*Exp.Date: Jun 30, 1986*

1a. REPORT SECURITY CLASSIFICATION
UNCLASSIFIED

1b. RESTRICTIVE MARKINGS

2a. SECURITY CLASSIFICATION AUTHORITY

2b. DECLASSIFICATION/DOWNGRADING SCHEDULE

3. DISTRIBUTION/AVAILABILITY OF REPORT
Distribution Limited

4. PERFORMING ORGANIZATION REPORT NUMBER(S)
06-5035

5. MONITORING ORGANIZATION REPORT NUMBER(S)

6a. NAME OF PERFORMING ORGANIZATION
Southwest Research Institute

6b. OFFICE SYMBOL *(If applicable)*

7a. NAME OF MONITORING ORGANIZATION
Dr. Steven G. Fishman — Code 431N
Office of Naval Research

6c. ADDRESS *(City, State, and ZIP)*
6220 Culebra Road, P.O. Drawer 28510
San Antonio, TX 78228-0510

7b. ADDRESS *(City, State, and ZIP Code)*
800 North Quincey Street
Arlington, VA 22217

8a. NAME OF FUNDING/SPONSORING ORGANIZATION
Office of Naval Research

8b. OFFICE SYMBOL *(If applicable)*

9. PROCUREMENT INSTRUMENT IDENTIFICATION NUMBER
N00014-92-C-0093

8c. ADDRESS *(City, State, and ZIP)*
800 North Quincey Street
Arlington, VA 22217

10. SOURCE OF FUNDING NUMBERS

| PROGRAM ELEMENT NO. | PROJECT NO. | TASK NO. | WORK UNIT ACCESSION NO. |
|---|---|---|---|
| | | | |

11. TITLE *(Include Security Classification)*
Characterization of Compressive Damage Mechanisms in Ceramic and Polymeric Matrix Composite Materials

12. PERSONAL AUTHOR(S)

13a. TYPE OF REPORT
Final

13.b TIME COVERED
FROM 10/93 TO 2/95

14. DATE OF REPORT *(Year, Month, Day)*
February 1995

15. PAGE COUNT

16. SUPPLEMENTARY NOTATION

17. COSATI CODES

| FIELD | GROUP | SUB-GROUP |
|---|---|---|
| | | |
| | | |

18. SUBJECT TERMS *(Continue on reverse if necessary and identify by block number)*
Key Words: polymeric composites; ceramic composites; compression; compressive damage; kinking; hydrostatic pressure; shear failure; fiber reinforcement; interfacial shear stress; debonding; strain rate

19. ABSTRACT *(Continue on reverse if necessary and identify by block number)*

Experiments involving expansion of the dynamic strain rate capabilities of the split Hopkinson pressure bar were performed. Unusually high strain rate hardening was obtained for the compressive failure of silicon nitride, while for silicon carbide, failure followed a lower rate of hardening, crack kinetics criterion. The silicon nitride results were interpreted in terms of plastic deformation, which changed the mode of failure from that observed at low strain rates, and altered the strength-strain rate dependency, apparently through the influence of dislocation generation upon microcrack nucleation.

Recent experiments involved the response of monolithic ceramics and fiber-reinforced ceramic matrix composites to dynamic loading under hydrostatic confinement. Curious results were obtained for monolithic ceramics, which appeared to derive from crack initiation/growth kinetics and the stability of confined microcrack ensembles. Composites under confinement were found to reflect both dilatational and shear aspects of damage development, which are primarily a function of the matrix phase, while the effect of the fibers was to alter the relative kinetics and, under certain circumstances, the sequence of events involved in the macroscale growth of damage through the eventual zone of failure.

Considerable effort has been devoted to new approaches to capturing the critical events associated with compressive kink band nucleation and development in polymeric matrix, fiber reinforced composites. Several promising approaches were developed, and the application of each to the problem is being pursued concurrently.

20. DISTRIBUTION/AVAILABILITY OF ABSTRACT
☒ UNCLASSIFIED/UNLIMITED ☐ SAME AS RPT. ☐ DTIC USERS

21. ABSTRACT SECURITY CLASSIFICATION
UNCLASSIFIED

22a. NAME OF RESONSIBLE INDIVIDUAL

22b. TELEPHONE *(Include Area Code)*
210/522-2317

22c. OFFICE SYMBOL

**DD FORM 1473** 84 MAR

83 APR edition may be used until exhausted.
All other editions are obsolete.

SECURITY CLASSIFICATION OF THIS PAGE

UNCLASSIFIED

# TABLE OF CONTENTS

# LIST OF FIGURES

Page

## I.
## High Strain Rate Compression and Plastic Flow of Ceramics

# LIST OF FIGURES (continued)

Page

## II.

## Utilization of the Split Hopkinson Pressure Bar Under Hydrostatic Confining Pressure to Characterize the Compressive Behavior of Ceramics and Ceramic Composites

## III.

## Failure of Fiber-Reinforced Ceramic Matrix Composites Under Dynamic Loading Conditions

## LIST OF FIGURES (continued)

## IV.
## Experimental Characterization of Kink Band Development in Polymeric Composites: A Report of Recent Progress

# FOREWORD

This document constitutes a Final Report of research into the mechanisms associated with compressive failure of fiber-reinforced ceramic and polymeric matrix composites. The report consists of three papers dealing with ceramic matrix composites, plus a report of work during the last year aimed at establishing several new approaches for characterizing certain aspects of compressive damage development peculiar to polymeric composites. These new techniques are expected for form the basis for continuing research on this class of composite.

*Journal of Materials Science (submitted)*

## I.

# HIGH STRAIN RATE COMPRESSION AND PLASTIC FLOW OF CERAMICS

By
J. Lankford
Southwest Research Institute
San Antonio, Texas 78228-0510

## ABSTRACT

Experiments involving expansion of the dynamic strain rate capabilities of the split Hopkinson pressure bar are described. Unusually high strain rate hardening is obtained for the compressive failure of silicon nitride, while for silicon carbide, failure follows a lower rate of hardening, crack kinetics criterion. The $Si_3N_4$ results are interpreted in terms of plastic deformation, which changes the mode of failure from that observed at low strain rates, and alters the strength-strain rate dependency, apparently through the influence of dislocation generation upon microcrack nucleation.

# I. INTRODUCTION

A number of studies have suggested that plastic deformation may, under certain circumstances, play an important role in the compressive failure of strong, nominally brittle ceramics at quite low homologous temperatures. These circumstances appear to include both shock loading[1-3] and quasistatic compression under high hydrostatic confinement.[4] Other work involving such conditions has focussed on the kinetics and micromechanics of the nucleation and growth of ensembles of microcracks[5-8] to explain observed trends in strength. The present objective is to note what seem to be several critical issues arising from these bodies of work, and to report on the results of new experiments aimed at shedding some light on the microplasticity versus microfracture question.

Ultimately, all ceramics fail in pure compression by the coalescence of a multitude of axially-oriented microcracks.[6-9] For low rates of loading ($10^{-5}$ $s^{-1}$ to $15^{-1}$), it has been shown[6-8] that this process obeys a relationship of the form

$$\sigma_c \propto \dot{\epsilon}^{1/(1+n)} \tag{1}$$

where $\sigma_c$ is the compression strength, $\dot{\epsilon}$ is the strain rate, and n is equal to the stress intensity exponent in the macroscopic tensile crack velocity relationship. Since n is a number ranging from 50 to 200, Eq. (1) describes a relatively strain rate-insensitive process, controlled by thermally-activated growth of microcracks. It is well-known that microstructural factors are responsible for the existence of local tensile stresses near grain boundaries and material inhomogeneities within ceramic bodies subject to nominally compressive uniaxial loads. The localized tensile fields serve to nucleate microcracks, which then grow subcritically. This process has been shown[6-8] to dominate the compressive failure of a number of ceramics ($Al_2O_3$, $Si_3N_4$, and SiC).

Higher rates of compressive loading have been achieved by utilizing the split Hopkinson pressure bar (SHPB) technique, whereby a rapidly rising stress pulse is produced within a specimen sandwiched between steel bars impacted by a gas-gun driven projectile. Under these circumstances, the dependence of strength upon strain rate for a number of brittle materials has been found to be considerably more robust.[6-8] Usually, however, the strain rate range available in such experiments has been limited to a small fraction of the decade above 1,000 $s^{-1}$, which makes accurate determination of the $\sigma_c \bullet \dot{\epsilon}$ relationship difficult.

Results to date have been interpreted as generally consistent with theoretical predictions based upon the idea[5] of crack inertia as a controlling factor in the dynamic tensile failure of brittle materials. This concept may be transposed to the case of compressive failure by recognizing that, as noted earlier, global compressive fields in real materials are resolved by microstructural constraints into a large population of local tensile enclaves. Given this proviso, the model of Grady and colleagues predicts[5,10,11] that there will be a transition from the dependence provided by Eq. (1) to one described by

$$\sigma_c \propto \dot{\epsilon}^{1/3} \tag{2}$$

This transition should occur[5] at a material-dependent characteristic strain rate that for most ceramics lies in the range $10^3$ $s^{-1}$ to $10^4$ $s^{-1}$.

Experimental studies performed at much higher strain rates have led to the conclusion, however, that while microfracture certainly is the eventual cause of failure, its occurrence may be affected by microplasticity. Cagnoux and Longy,[1,2] for example, investigated the response of both glass-ceramic and sintered alumina to high strain rates ($\geq 10^6$ $s^{-1}$) and high stresses in excess of the Hugoniot elastic limit via high velocity plate impacts. The alumina was characterized by glassy second phase grain boundaries, while the boundaries of the glass-ceramic crystallites were simply amorphous. Based on TEM and X-ray diffraction analysis of recovered samples, it was concluded that in the case of the glass-ceramic, microplasticity begins to occur at stresses as low as 0.6 HEL, and appear to be the direct cause of microcrack nucleation at the crystallite-glassy phase interface. Similarly, for the alumina with extensive glass phase, microplasticity is first observed below the HEL, and is accompanied by microcracking of the intergranular glass phase. When the grain boundary phase is minimal (99.7% $Al_2O_3$), however, plasticity without associated microfracture is observed from 0.9 HEL to 2.0 HEL.

Clearly, the idea that emerges here is that blocked plastic flow induces grain boundary stress concentrations and associated microfracture. If, on the other hand, grain boundaries are relatively clean, slip may be nucleated in adjacent grains, relaxing dislocation pileup stresses. Results of Beauchamp's study[3] of densification of pure alumina powder subject to shock loading appear to support this concept, in that the free particles densify by pure plastic deformation, with virtually no particle microfracture.

Most recently, Sharma, *et al.*,[12,13] have performed an unusual series of dynamic fatigue experiments involving two different types of silicon nitride. One of these had an amorphous grain boundary phase, and the other a predominantly crystalline grain boundary phase. The materials were tested under repeated compressive impact loading, whereby the strain rate corresponding to the impulsive load in a split Hopkinson pressure bar (SHPB) was about 500 $s^{-1}$. It was found that dislocation activity increased in both materials with the accumulation of stress pulses, but the amorphous grain boundary phase also blocked dislocations. Very limited data suggested that this was reflected in a slightly greater fatigue life at a given impact stress level for the latter material.

The flyer plate, shock loading, and dynamic fatigue experiments outlined above all indicate that plastic flow occurs in ceramics under the conditions described, and that grain boundary microstructure influences both deformation and associated microfracture. However, none of the studies have dealt effectively with the issue of whether there exists a link between this phenomenon and the key physical property, strength. Consequently, the objective of the present work is to determine whether microstructural mediation of plastic flow can have a significant effect on the uniaxial compressive strength of strong ceramics at high loading rates. In order to accomplish this goal, it was necessary to develop a means of expanding the SHPB strain rate regime so as to generate a valid strength versus strain rate dependence.

## II. EXPERIMENTAL PROCEDURES

### A. Materials

Two high strength ceramics were chosen for use in the study, one a silicon carbide characterized by exceptionally "clean" grain boundaries, the other a silicon nitride processed so as to yield an amorphous second phase grain boundary film. Compositions and properties of the sintered alpha-phase SiC and the hot-pressed $Si_3N_4$ are shown in Table I.

Cylindrical test samples (1.25 cm long x 0.625 cm diameter) were machined from the as-processed billets, with their ends ground and polished parallel within 5 μm. Platens of ultra high strength aluminum oxide, likewise ground and polished parallel to the same tolerance, were prepared for use as compressive loading inserts. Procedures used have been presented in detail elsewhere.[6-8]

### B. Low/Intermediate Strain Rate Experiments

Low strain rate compression testing was performed using a servo-controlled hydraulic test machine. Tests were run to failure at strain rates of approximately $10^{-5}$ $s^{-1}$ and $1 s^{-1}$.

### C. High Strain Rate Experiments

In order to achieve a wider dynamic strain rate range, modifications were implemented into the split Hopkinson pressure bar test procedures. First, it should be noted that the pressure bar stress pulse is generated by the transfer of momentum from a gas-gun driven steel projectile (striker) usually traveling around 30 m/s (Figure 1). The rate of momentum transfer into the pressure bar system, hence the slope of the load-time pulse, is determined by the closure rate of the slightly rounded face of the striker against the flat end surface of the incident pressure bar. By increasing the velocity of the striker, the rate of energy transfer is thereby increased, with a corresponding rise in strain rate, as shown for a series of calibration shots in Figure 2.

Recently, it was observed,[14] and subsequently predicted theoretically,[15] that for most ceramics, stress wave dispersion within the transmitter pressure bar will begin to manifest itself at a true strain rate (within the specimen as determined by a strain gage) of about 2,700 $s^{-1}$. This also was found to be true in the present case, as shown in Figure 3. Accordingly, sample-mounted strain gages rather than the usual transmitter bar signals were relied on for measuring strain rates (Figure 4). Using this technique, specimen strain rates in the range of 2,000 $s^{-1}$ to 5,000 $s^{-1}$ could be attained, as shown in the latter figure.

To extend the test regime still further, relatively soft 6061-T6 Al metal spacers were placed on the face of the incident bar that was impacted by the striker. The resulting incident pulse rise time is then governed by the rate of plastic flow within, hence the thickness of, the spacer (Figure 5). By this means, similar to that recently employed by Sharma, *et al.*,[12] in their dynamic fatigue experiments, incident bar strain rates ranging from 200 $s^{-1}$ to 700 $s^{-1}$ were attained, as shown in Figure 6.

## D. Characterization of Failure Mechanisms

Debris from failed samples was collected, mounted on SEM stubs, and coated with palladium. Fractographic features were then characterized using scanning electron microscopy.

# III. RESULTS

Compressive strength behavior for SiC and $Si_3N_4$ is shown over the entire strain rate range in Figures 7 and 8. For silicon carbide, strength is virtually constant at 4,000 MPa until a strain rate of about 800 $s^{-1}$ is attained, at which point $\sigma_c$ begins to rise rapidly. Similarly, the strength of hot pressed $Si_3N_4$ increases slowly over some eight decades in strain rate, before accelerating (even more rapidly than did the SiC) beyond $\dot{\epsilon} \cong 2,000\ s^{-1}$.

The dynamic strengthening regimes are expanded in Figures 9 and 10. In the case of the silicon carbide (Figure 9), a best-fit curve through the data is found to obey a relationship of the form

$$\sigma_c \propto \dot{\epsilon}^{0.31} \tag{3}$$

Silicon nitride, on the other hand, behaves in a significantly different manner, whereby

$$\sigma_c \propto \dot{\epsilon}^{0.87} \tag{4}$$

while the SiC results are basically compatible with the crack kinetics (cube root of the strain rate) model (Eq. (2)), it is clear that the $Si_3N_4$ data are not.

Representative scanning electron micrographs obtained from typical sample fragments are shown in Figure 11. For all strain rates, microfracture in SiC occurred by a mixed mode (transgranular/intergranular) process (Figures 11a and 11b). Silicon nitride again behaved differently. At all strain rates below the transition at $\dot{\epsilon} \simeq 2{,}000\ s^{-1}$, the fracture surface was characterized by faceted, transgranular features (Figure 11c), attended by extensive sub-grain size "debris" that appeared to be part of the surface, i.e., it was attached,* thus representing some sort of microcrack tortuosity. Above the strength-strain rate transition, the failure of $Si_3N_4$ was clearly of a predominantly intergrancular character (Figure 11d), although the fracture surface again was partly covered by attached microfragments on a sub-grain size scale.

## IV. DISCUSSION

The preceding results suggest that the responses of $Si_3N_4$ and SiC to compressive loading in the strain rate range 800 $s^{-1}$ to 4,000 $s^{-1}$ differ in a fundamental way. In the case of SiC, it appears that the material transitions under dynamic loading to a failure criterion that is at least dominated

---

* Ultrasonic cleaning in alcohol failed to dislodge the microfragments.

by crack kinetics. That is, the data shown in Figure 9, described empirically by a strain rate exponent of 0.31, deviate only slightly from a cube root dependence. Moreover, the fractography results indicate that the same physical microfracture events are occurring under both quasistatic and dynamic stress conditions.

The inferred role of crack velocity is supported by earlier experiments[16] in which fragment size distributions were obtained for a series of compression tests performed using the same silicon carbide at strain rates of $10^{-4}$, $10^{6}$, and $2.2 \times 10^{3}$ $s^{-1}$. It was found that for the latter rate, the average fragment size decreased dramatically relative to those measured for both lower strain rate conditions. Dynamic fragment dimensions were in excellent agreement with theoretical predictions by Grady and Kipp[5] derived purely on the basis of microcrack kinetics.

The strength-strain rate dependence obtained for the failure of silicon nitride under dynamic loading clearly is incompatible with this picture. No current theory of the fracture of monolithic ceramics under such conditions predicts a strain rate exponent of 0.87. However, it is possible to rationalize this behavior on the basis of prefailure microplasticity.

A higher (than predicted by crack kinetics) strain rate exponent implies that the effect of faster loading is to suppress fracture initiation. Clearly, such initiation may have a multiplicity of potential microstructural origins, i.e., grain boundary pores, grain boundary ledges, and triple points. Moreover, hot-pressed $Si_3N_4$ is a two-phase material, which in itself creates stress localizations at sites of $\alpha$-$\beta$ grain impingement due to elastic moduli mismatch.

Because of those stress concentrations, it is likely that localized plastic flow is initiated as postulated by Sharma, *et al.*[12,13] At low strain rates, subcritical crack nucleation beginning at moderate stresses occurs below the level required to generate dislocations. By the time high stresses are reached, and a few dislocations nucleate, the sample is close to failure, which occurs for both SiC and $Si_3N_4$ via the coalescence of numerous microcracks that have been growing subcritically.

The picture changes at high rates of loading. High stresses are reached quickly, and subcritical crack nucleation and growth are suppressed according to the crack kinetics criterion. Moreover, dislocation nucleation and associated microcrack initiation now can compete at local stress concentrators with pure crack nucleation. From Table I, it can be seen that the hardness, hence the closely related yield strength (about $\frac{H}{2.1}$ for most strong ceramics[17]) for SiC is considerably higher than for $Si_3N_4$. Thus, slip band nucleation will be more difficult than for $Si_3N_4$, and pure crack-nucleated failure, according to Eq. (2), would be more favored, as is observed is Eq. (3). Moreover, since no grain boundary phase is present in the SiC, the grain boundaries would be relatively transparent to slip in adjacent grains, thereby relaxing dislocation pileups and mitigating microfracture.

For silicon nitride, on the other hand, plastic flow will be facilitated by its lower yield strength; for this material, $\frac{H}{2.1}$ is about 8.5 GPa, which in turn corresponds to a shear strength of approximately 6.1 GPa. A grain boundary stress concentration of only about 1.5 would be required to generate local shear stresses of this magnitude at applied compressive stresses of 4.0 GPa, the onset of the rapid hardening regime. With increasing strain rate, crack nucleation will be inhibited by the combination of crack inertia (Eq. (2)), plus the finite (sound speed limited) rate at which dislocation pileups can form in order to nucleate cracks. These can initiate in a variety of ways (Figure 12), depending on the particular combination of slip band, grain boundary, and potential cleavage plane orientations, as well as the surface engines associated with the latter, i.e., intracrystalline cleavage (1, 2 in Figure 12), intergranular microfracture (3), or slip band cleavage. At high loading rates in $Si_3N_4$, the grain boundary phase appears consistently to be the weak link in this scenario, producing intergranular failure at the site of blocked slip bands. This is consistent with the dynamic cyclic fatigue results of Sharma, *et al.*[12]

## V. CONCLUSIONS

It is found that the dynamic compressive failure of hot-pressed silicon nitride contrasts with that of sintered silicon carbide. The results can be rationalized in terms of purely brittle dynamic microfracture in the case of SiC, and plastic flow-initiated microcracking in $Si_3N_4$.

## ACKNOWLEDGEMENTS

The excellent experimental work performed by Mr. Arthur Nicholls is acknowledged with appreciation. The support of the Office of Naval Research under Contract No. N00014-92-C-0093 is gratefully acknowledged.

## REFERENCES

1. Longy, F., and Cagnoux, J., "Plasticity and Microcracking in Shock-Loaded Alumina," *J. Am. Ceram. Soc.*, **72**, 971-979 (1989).

2. Cagnoux, J., and Longy, F., "Spallation and Shock-Wave Behavior of Some Ceramics," *J. de Physique*, **49**, C3-C9 (1988).

3. Beauchamp, E. K., Carr, M. J., and Graham, R. A., "Plastic Deformation in Alumina by Explosive Shock Loading," *J. Am. Ceram. Soc.*, **68** [12], 696-699 (1985).

4. Heard, H. C., and Cline, C. F., *J. Mat. Sci.*, **15**, 1889-1897 (1980).

5. Grady, D. E., and Kipp, M. E., "The Micromechanics of Impact Fracture of Rocks," *Int. J. Rock Mech. Min. Sci. Geomech. Abstr.*, **16**, 293-302 (1979).

6. Lankford, J., "The Role of Tensile Microfracture in the Strain Rate Dependence of Compressive Strength of Fine-Grained Limestone — Analogy with Strong Ceramics," *Int. J. Rock Mech. Min. Sci. Geomech. Abst.*, **18**, 173-175 (1981).

7. Lankford, J., "Mechanisms Responsible for Strain-Rate-Dependent Compressive Strength in Ceramic Materials," *J. Am. Ceram. Soc.*, **64** [2], C-33-C-34 (1981).

8. Lankford, J., "The Role of Subcritical Tensile Microfracture Processes in Compressive Failure of Ceramics," to be published in *Fracture Mechanics of Ceramics*, edited by R. C. Bradt, A. G. Evans, D.P.H. Hasselman, and F. F. Lange, Plenum, NY.

9. Lankford, J., "The Compressive Strength of Ceramics: Microplasticity Versus Microfracture," *J. Hard Materials*, **2**, 55-77 (1991).

10. Grady, D. E., and Lipkin, J., "Criteria for Impulsive Rock Fracture," *Geophys. Res. Lett.*, **7**, 255-258 (1980).

11. Grady, D. E., and Hollenback, R. E., "Rate-Controlling Processes in the Brittle Failure of Rock," Tech. Report. SAND 76-0659, February 1977, pp. 62.

12. Sharma, V., Vecchio, K. S., and Nemat-Nasser, S., "Fatigue in Silicon Nitride, Part I: Effect of Grain Boundary Phase on Dynamic Compression Fatigue in Hot-Pressed Silicon Nitride," *J. Am. Ceram. Soc.* (in press).

13. Sharma, V., Vecchio, K. S., and Nemat-Nasser, S., "Fatigue in Silicon Nitride, Part II: Damage Evolution in Hot-Pressed Silicon Nitride Under Quasistatic Compression Fatigue," *J. Am. Ceram. Soc.* (in press).

14. Staehler, J. M., Predebon, W. W., Pletka, B. J., and Lankford, J., "Testing of High-Strength Ceramics with the Split Hopkinson Pressure Bar," *J. Am. Ceram. Soc.*, **76** [2], 536-538 (1993).

15. Ravichandran, G., and Subhash, G., "Critical Appraisal of Limiting Strain Rates for Compression Testing of Ceramics in a Split Hopkinson Pressure Bar," *J. Am. Ceram. Soc.*, 77, 263-267 (1994).

16. Lankford, J., and Blanchard, C. R., "Fragmentation of Brittle Materials at High Rates of Loading," *J. Mat. Sci.*, **26**, 3067-3072 (1991).

17. Johnson, K. L., "The Correlation of Indentation Experiments," *J. Mech. Phys. Solids*, **18**, 115-126 (1970).

# TABLE I
# MATERIAL PROPERTIES

| Material | Flexural Strength (MPa) | Hardness (GPa) | Fracture Toughness ($MNm^{-3/2}$) | Grain Size (μm) |
|---|---|---|---|---|
| $\alpha$ - SiC | 345 | 28 | 4.4 | 3-5 |
| HP $Si_3N_4$ | 490 | 17.8 | 5.4 | 0.5-3 |

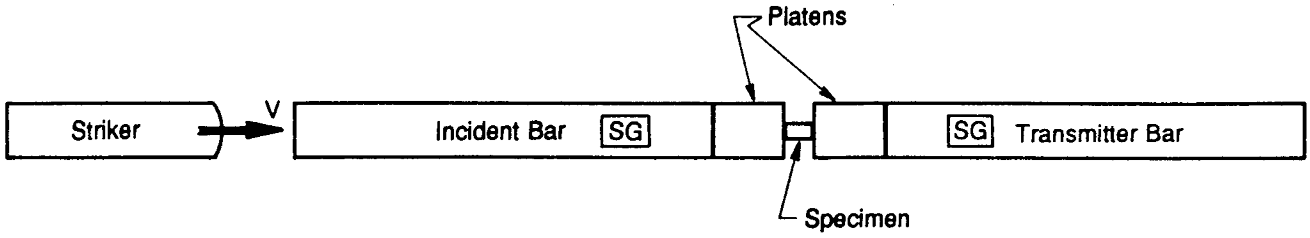

Figure 1. Schematic of Split Hopkinson Pressure Bar.

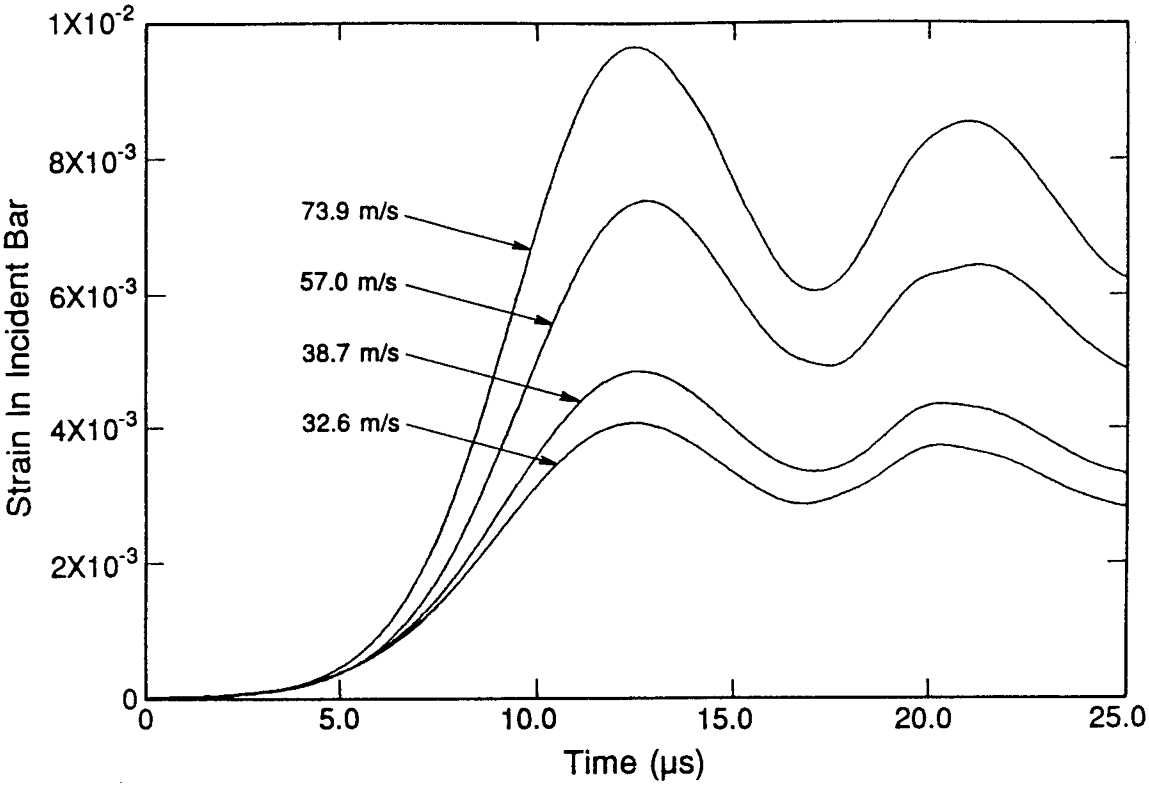

Figure 2. Strain in incident pressure bar versus rise time for varying striker velocity, showing increase in strain rate with velocity.

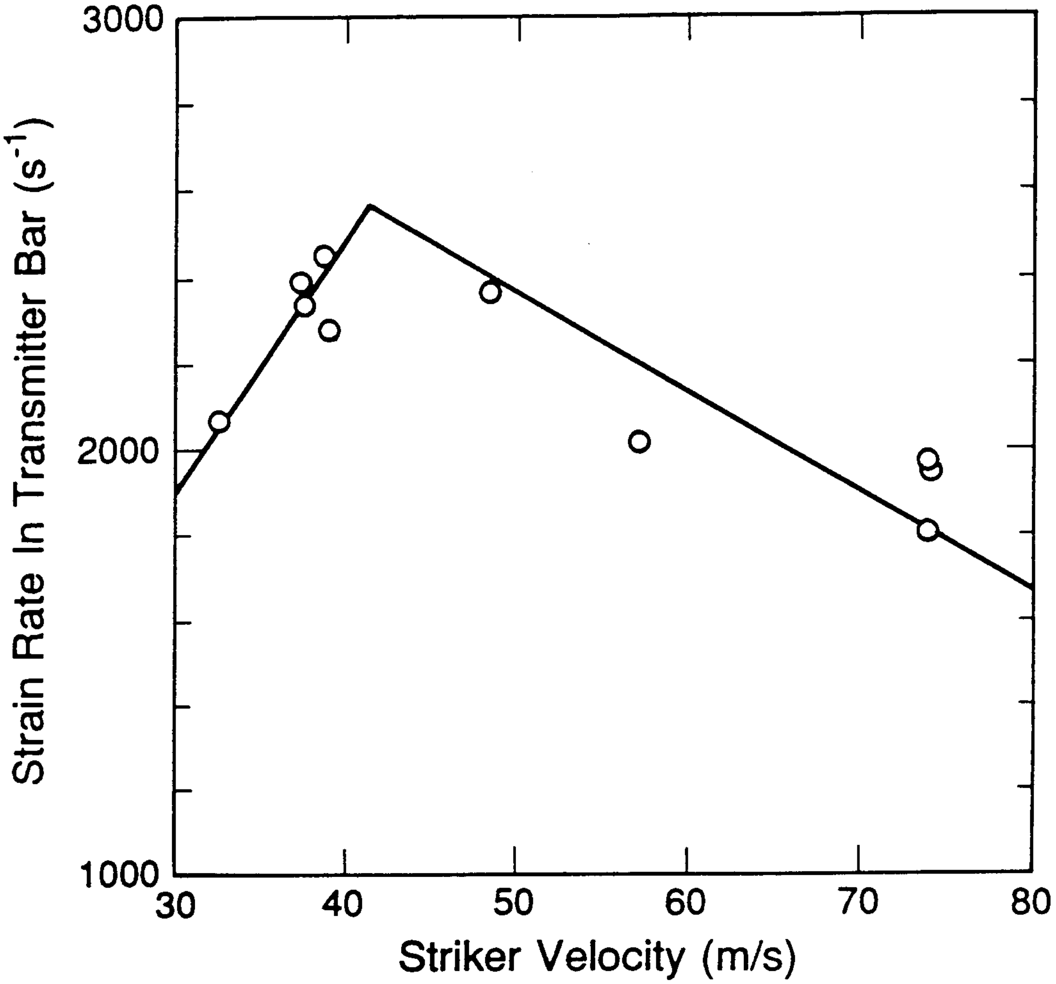

Figure 3. Strain rate in transmitter pressure bar versus striker velocity, showing dispersion-induced decline in strain rate above critical value.

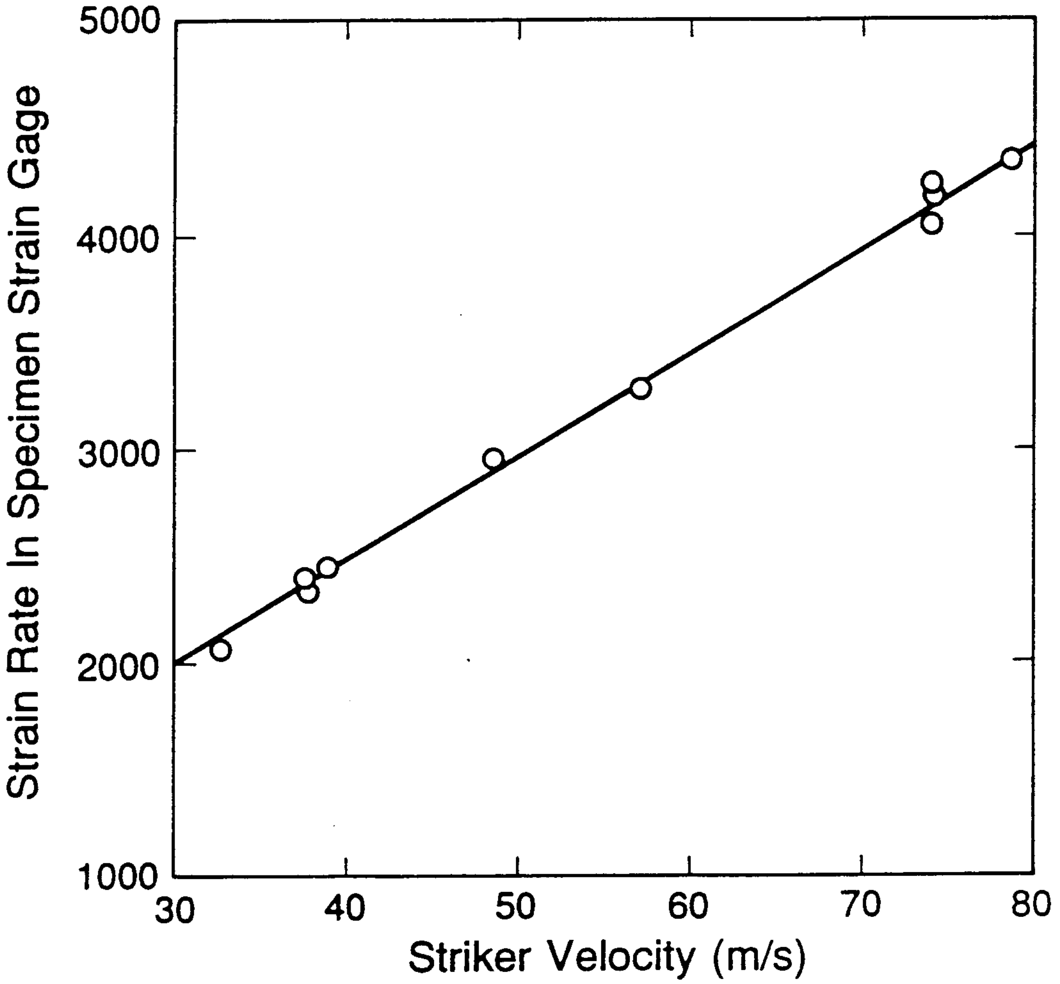

Figure 4. Strain rate in specimen versus striker velocity.

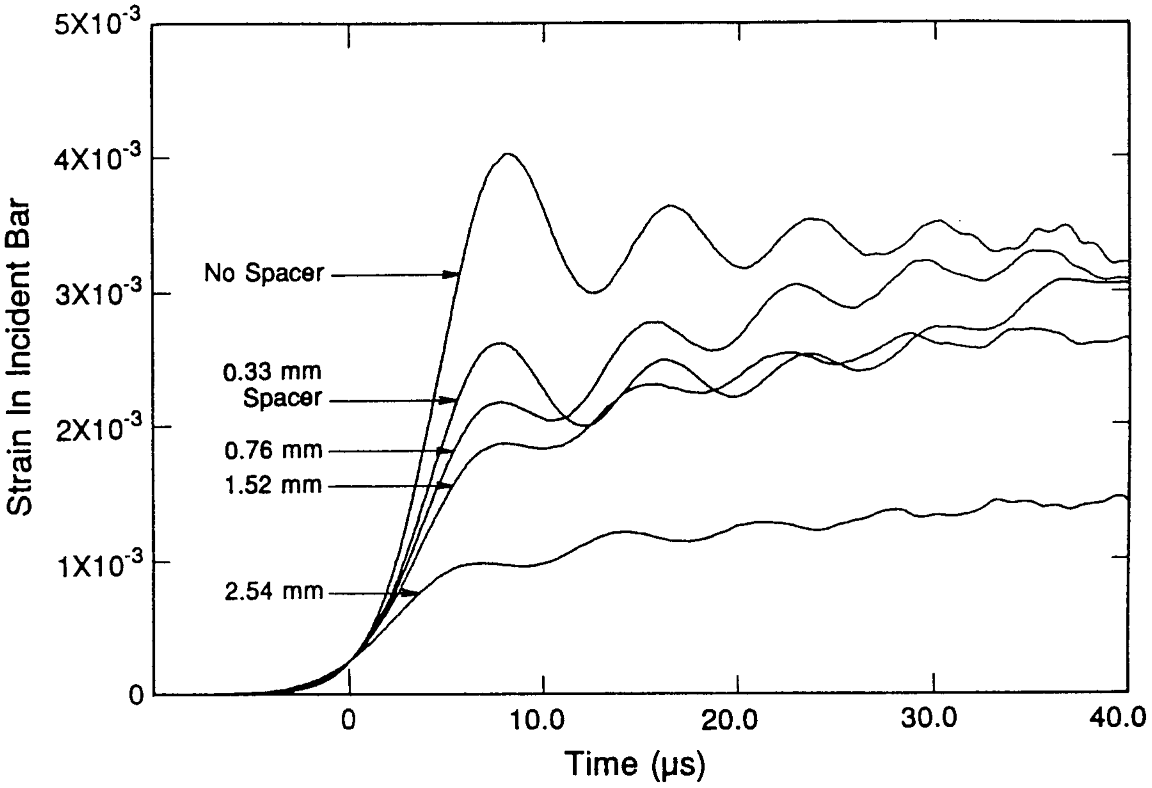

Figure 5. Pulse records in the incident pressure bar resulting from the impact of a striker traveling at 33 m/s with and without 6061-T6 Al spacers of varying thickness, showing increase in strain rate with decreasing spacer thickness.

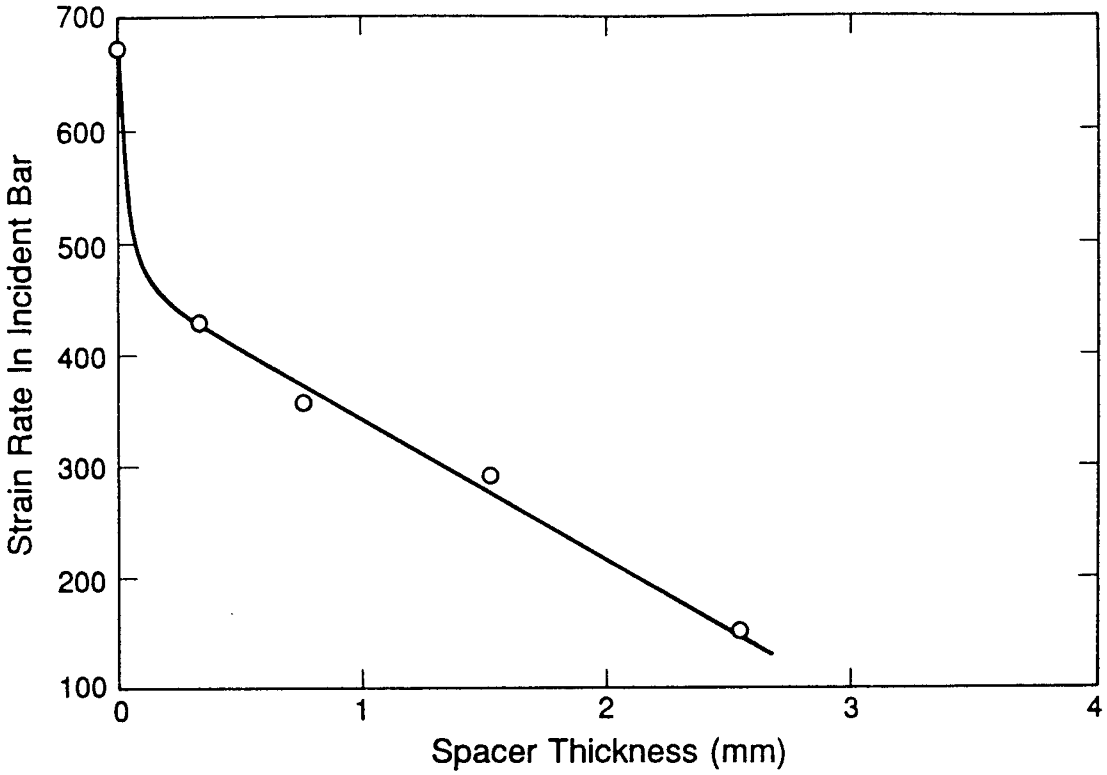

Figure 6. Strain rate in incident pressure bar versus spacer thickness.

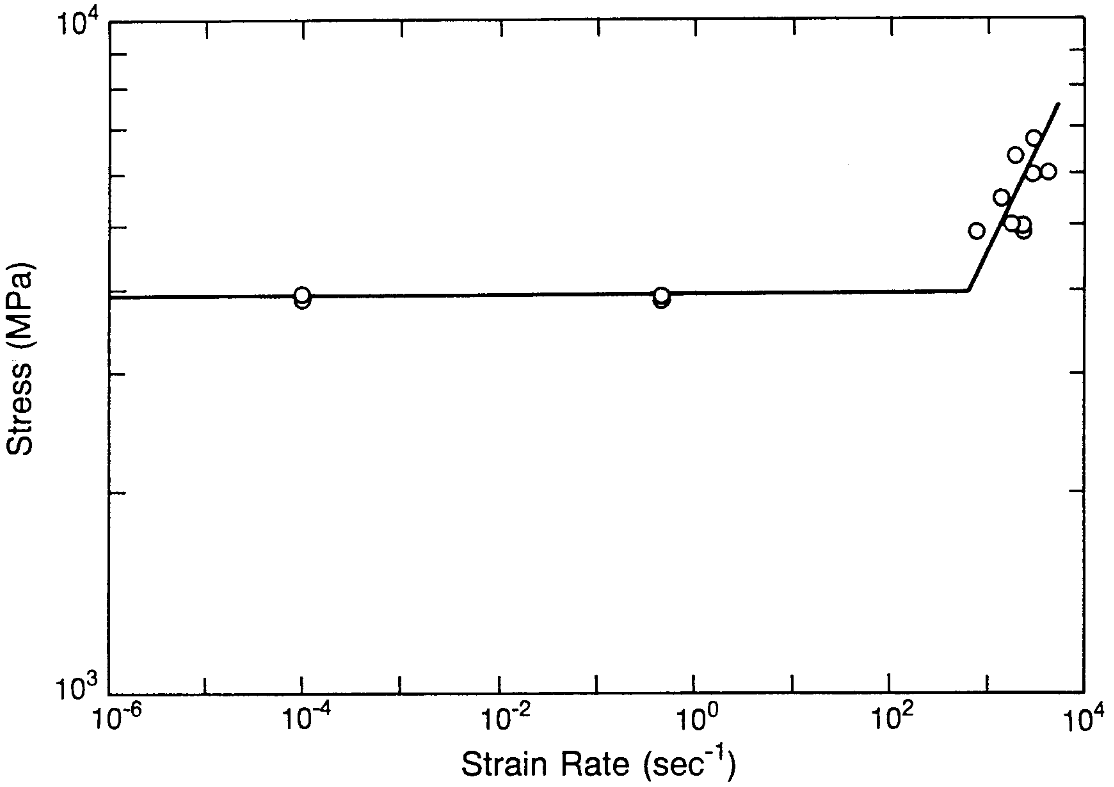

Figure 7. Compressive strength versus overall strain rate range for sintered silicon carbide.

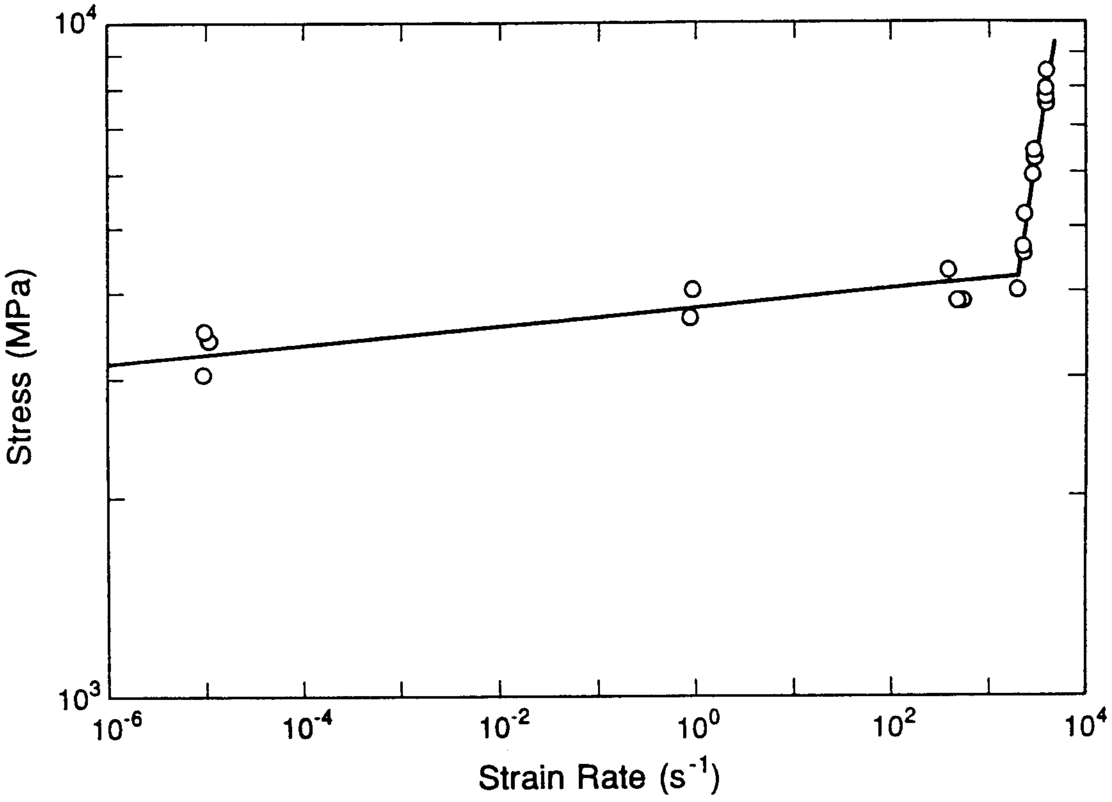

Figure 8. Compressive strength versus overall strain rate range for hot-pressed silicon nitride.

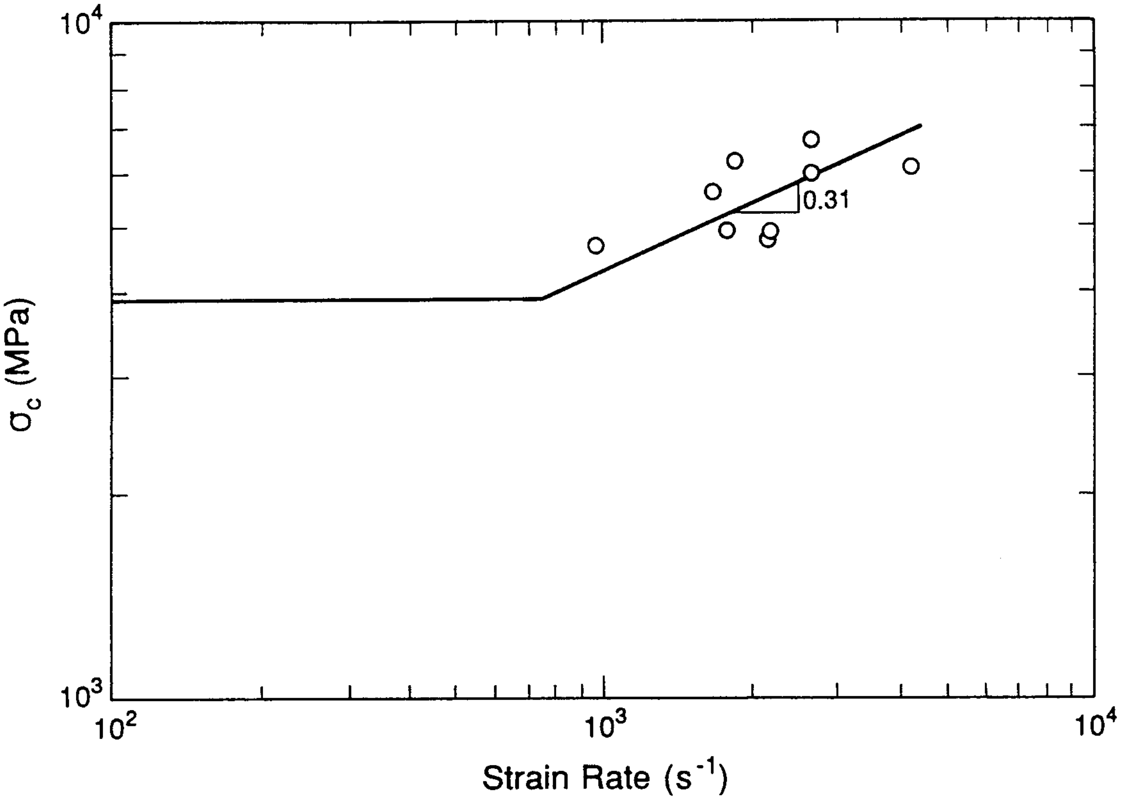

Figure 9. Compressive strength versus dynamic strain rate for SiC.

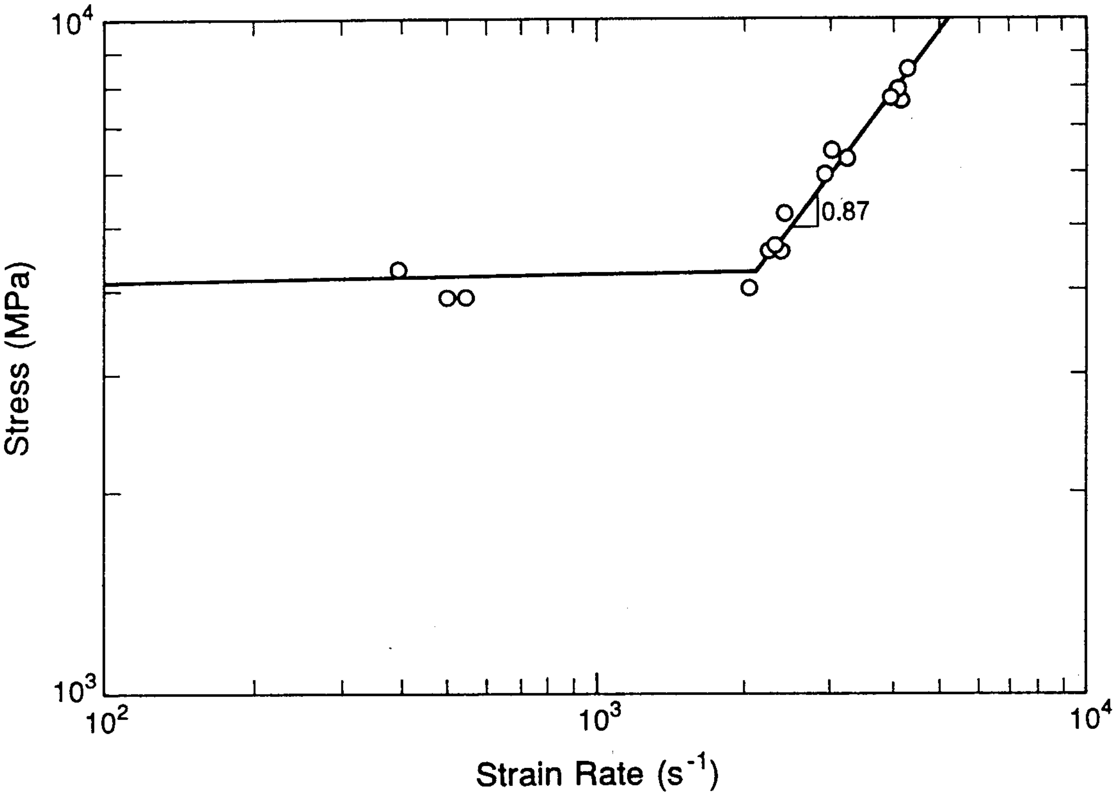

Figure 10. Compressive strength versus dynamic strain rate for hot-pressed silicon nitride.

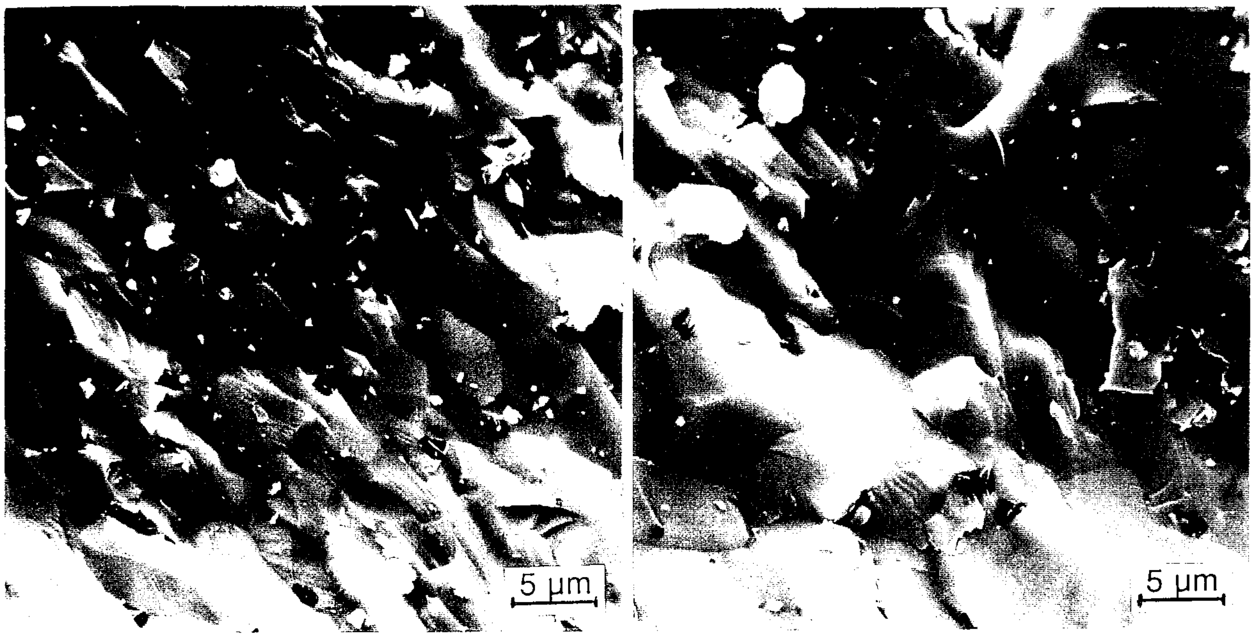

(a) SiC, $\dot{\epsilon} = 10^{-4}$ s$^{-1}$. (b) SiC, $\dot{\epsilon} = 2{,}100$ s$^{-1}$.

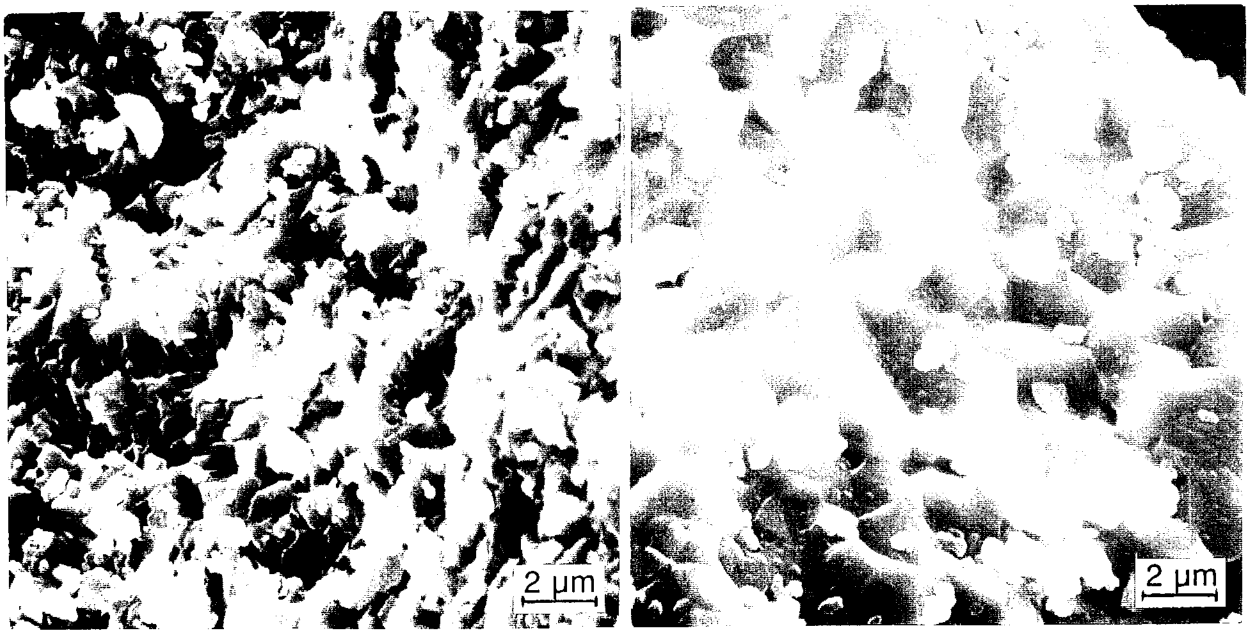

(c) $Si_3N_4$, $\dot{\epsilon} = 10^{-4}$ s$^{-1}$. (d) $Si_3N_4$, $\dot{\epsilon} = 2{,}950$ s$^{-1}$.

Figure 11. Fractographic detail from compressive test fragments.

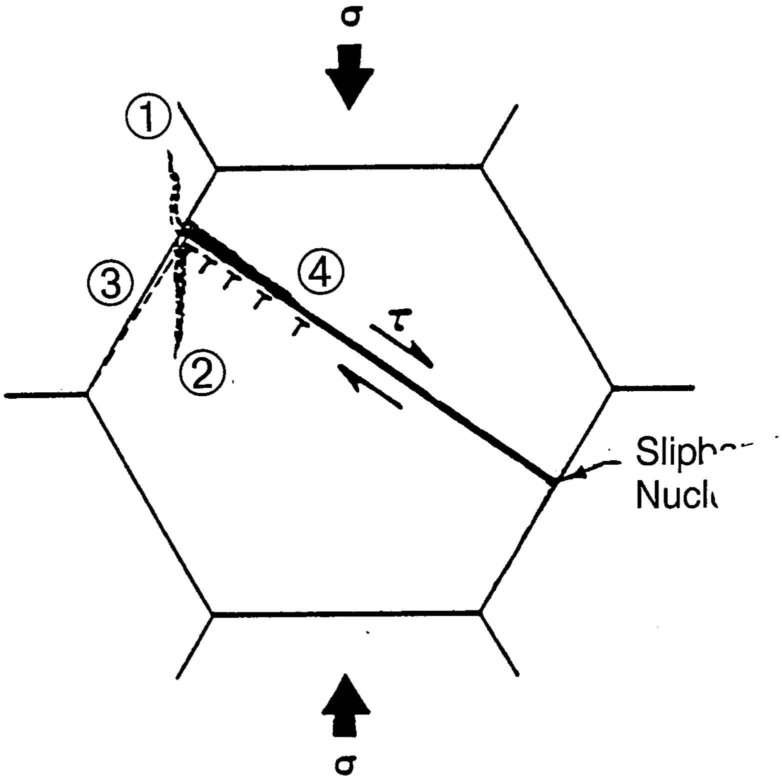

Figure 12. Geometry of compressive slip band-nucleated intracrystalline cleavage (1,2), intergranular separation (3), and slip band microfracture (4).

Published in: *Mechanical Testing of Ceramics and Ceramic Composites*,
ed. A. Gilat, TMS AIME, NY, pp. 1-10, 1994

## II.

# UTILIZATION OF THE SPLIT HOPKINSON PRESSURE BAR UNDER HYDROSTATIC CONFINING PRESSURE TO CHARACTERIZE THE COMPRESSIVE BEHAVIOR OF CERAMICS AND CERAMIC COMPOSITES

**James Lankford, Jr.**
Materials Engineering Department
Southwest Research Institute
San Antonio, Texas

## ABSTRACT

The behavior of brittle materials under dynamic loading conditions has been a subject of intense study, as has their behavior under multiaxial states of stress. However, it has proven to be a challenge to obtain data which reflect the influence of both factors simultaneously. One way to do so is to apply hydrostatic pressure to samples loaded axially by means of the split Hopkinson pressure bar. This paper reports on such experiments involving the compressive failure of monolithic ceramics and fiber-reinforced ceramic matrix composites. Problems associated with performing the experiments are outlined. Curious results are obtained for monolithic ceramics, which appear to derive from crack initiation/growth kinetics and the stability of confined microcrack ensembles. Composites under confinement can reflect both dilatational and shear aspects of damage development, which are primarily a function of the matrix phase, while the effect of the fibers is to alter the relative kinetics and under certain circumstances the sequence of events, involved in the macroscale growth of damage through the eventual zone of failure.

## INTRODUCTION

Depending upon the microstructure of a brittle material, its failure under compressive loading may reflect a combination of, or dominance by, dilatational and shear damage modes. Often their relative contributions can be difficult to separate and define; confined compression experiments, however, provide a seemingly ideal vehicle for making this assessment. As shown in Figure 1, the expansion of a cylindrical specimen due to an axial stress $\sigma_1$ is counteracted by the radial stress $\sigma_3$. Moreover, the shear stress in the cylinder, for given values of $\sigma_1$ and $\sigma_3$ is

$$\tau = (\sigma_1 - \sigma_3) \sin \theta \cos \theta \qquad (1)$$

where $\sigma_1 - \sigma_3$ is the compressive stress within the material relative to the hydrostat, and $\theta$ is the angle which the plane of initial failure makes the direction of $\sigma_1$. If $\sigma_1$ represents the flow or failure stress for various values of

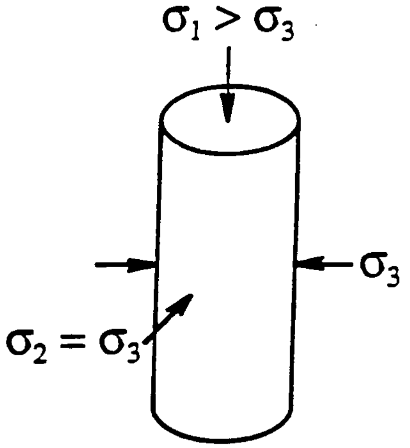

FIGURE 1. SCHEMATIC OF STRESS DISTRIBUTION RELATED TO COMBINED HYDROSTATIC PRESSURE-COMPRESSION TESTING.

$\sigma_3$, the relative influence of shear versus dilatation can be determined by plotting $\sigma_1 - \sigma_3$ versus $\sigma_3$. To the extent that relatively small changes in $\sigma_3$ create large increases in $\sigma_1 - \sigma_3$, dilatational crack initiation and/or growth mechanisms probably are involved. Conversely, the absence of pressure sensitivity in $\sigma_1 - \sigma_3$ (*i.e.*, a horizontal plot) would indicate that the strength (flow or failure) is controlled solely by a critical shear stress criterion. For a composite, this critical value is not necessarily the maximum macroscopic shear stress, as is generally found to be the case for isotropic, homogeneous materials, but may relate to a certain angle of bend in the reinforcing fibers required to fracture them in local tension, and thereby produce a propagating kink band.

A number of investigators have demonstrated that confinement can have a major effect on the strength of brittle monolithic materials; this has been shown for both rocks(1-4) and ceramics.(5,6) In particular, the compressive failure strength generally increases significantly with confining pressure, a dependence that can be interpreted to establish empirically the relevant failure criterion for a given material. It is known that in these cases the effect of pressure is manifested physically in the closure of axial microcracks, the coalescence of which ultimately causes compressively loaded specimens to fail.

Another factor which can affect fracture mode is the rate of load application. Thus, compressive strength tests performed at varying strain rates for several technological ceramics(7) indicate that for $\dot{\epsilon} > 10^2 s^{-1}$, some of the materials (SiC and hot-pressed $Si_3N_4$) exhibit a marked strain rate strengthening whereby

$$\sigma_c \propto \dot{\epsilon}^n \qquad (2)$$

where n > 0.3; for others (reaction-bonded $Si_3N_4$, Mg PSZ), no such strengthening is observed. These results suggest that there may exist a threshold strain rate for dynamic hardening which varies from one material to another. The most generally accepted rationalization for strain-rate strengthening of brittle materials is based on fracture kinetics considerations.

In particular, dynamic fracture mechanics has been utilized by Grady(8) and Grady and Hollenbach(9) to show that the tensile failure stress is given by:

$$\sigma_t = 3\sqrt{\rho_0 c_0 K_{IC}^2\, \dot{\epsilon}^{1/3}} \tag{3}$$

where $\rho_0$ is the density, $c_0$ is the wave speed, and $K_{IC}$ is the fracture toughness. Grady and Hollenbach(9) note that this relationship should hold for compression as well, since compressive failure is basically the result of the nucleation and growth of (locally) tensile microcracks. Thus, it would be expected that $\sigma_c$ likewise should be proportional to $\dot{\epsilon}^{1/3}$.

The lower bound strain rate $\dot{\epsilon}_*$ is predicted(10,11) to correspond to

$$\dot{\epsilon}_* = \frac{K_{IC}}{\rho_0 c_0 r_0^{3/2}} \tag{4}$$

where $r_o$ is the initial crack size. Substituting appropriate values of $\rho_0$, $c_0$, $r_0$, and $K_{IC}$ for ceramics yield $10^3 < \dot{\epsilon}_* < 10^4\, s^{-1}$.

By comparison with the preceding, relatively low equivalent work has been performed in the case of fiber-reinforced composites. Basically, the influence of dynamic strain rate has been investigated for SiC-fiber reinforced glass-ceramic(12) and for a carbon-fiber reinforced thermoplastic.(13) It was found that within the rapid loading regime, compressive strength was directly proportional to strain rate, and observed directly that at low strain rates, the polymeric composite failed by the nucleation and propagation of kink shear bands. Based on these facts, plus a simple model of dynamic shear band propagation which predicted $\sigma_c \propto \dot{\epsilon}^{1.0}$, it was inferred that a shear band process was responsible for the robust strain rate sensitivity.

Research on brittle materials in which both confining pressure and strain rate are varied in combination has been limited to rocks.(3,4,14) In the following sections, the results of a study aimed at exploring these effects for a monolithic ceramic and a fiber-reinforced ceramic matrix composite are presented.

## EXPERIMENTAL

### Materials

The material system selected for study was based on Compglas[1], i.e., SiC fiber reinforced lithium-alumino-silicate, a fine-grained glass ceramic. To represent the unreinforced matrix, a commercially-available pyroceramic[2] similar in chemistry and grain size (0.5-2.0 μm) was used.

### Specimen Preparation

Solid specimens were prepared for compression testing by fabricating the as-received material into right circular cylinders 12.5 mm long by 6.25 mm diameter. Loading faces were ground parallel within a tolerance of 4 μm, and then lapped smooth through 1 μm diamond. Loading platens of ultra high strength fine-grained alumina were prepared according to the same criteria.

Composite samples were prepared similarly, except that they had a slight waist which insured that failure occurred within the specimen gage section. To prevent their "brooming" at the sample-platen interface, the ends of the specimens were fitted with shallow end gaps, the cap between the sample and the inner wall of the caps being filled with epoxy.

---

[1] United Technologies Research Center, Middletown, CT.

[2] 9606, Corning Glass Works, Corning, NY

## Test Procedures

Low strain rate tests were performed at approximately $10^{-4}$ and $1s^{-1}$, with a servo-controlled hydraulic ram supplying the axial load. For tests with radial confining pressure, a special pressure vessel (690 MPa capacity) was utilized. In these experiments, the hydrostatic pressure was first raised to the desired level by pumping fluid into the pressure vessel while a servo-controller matched the axial stress to the pressure. Then the axial load was increased under displacement control at fixed pressure. A bridge of four electrical resistance strain gages inside the pressure vessel measured the axial load. Since the hydrostatic pressure produced a zero shift in the output of this load cell, the magnitude of the shift was measured in a series of calibration runs and subtracted from the load measurements. Hydrostatic pressure was measured by a diaphragm-type electric pressure transducer located at the fluid inlet orifice of the pressure vessel. The exact value of the strain rate, $\dot{\epsilon}$, was determined by measuring the stress rate, $\dot{\sigma}$, and calculating $\dot{\epsilon}$ using the appropriate value for Young's modulus, E, for each material, *i.e.*, $\dot{\epsilon} = \dot{\sigma}/E$. All samples were tested at room temperature. Specimens were sealed within thin, heat-shrinkable Teflon tubing, overlapping the small ends of the platens in order to prevent the silicon-based pressure fluid from infiltrating surface ores and causing premature failure.

Tests at strain rates in excess of $1000s^{-1}$ were performed using a split Hopkinson pressure bar (SHPB) apparatus initially developed for the testing of ductile materials, which has been described in detail elsewhere. The required impact velocities and stresses are achieved by using a pneumatically-driven projectile (impacting bar) guided by a long launch tube. Maximum impact velocities are of the order of 100 m/s, limited by the maximum yield stress in the pressure bars. These bars are composed of maraging steel tempered to a yield stress of approximately 2500 MPa.

The collision of the striker bar gives rise to a stress pulse which is twice the length of the striker bar and travels down the bar with a wave speed of $(E/\rho)^{1/2}$, where E is the elastic modulus and $\rho$ is the density. When this pulse comes to the end of the incident steel bar, it is partially reflected back up the bar and partially transmitted into the specimen. As the diameter of the bar is greater than the diameter of the specimen, there is also a stress multiplication factor equal to the ratio of the cross-sectional area of the bar to the cross-sectional area of the sample. For the case described above, this gives rise to a stress amplification of four. The stress pulse undergoes numerous reflections inside the sample as it reflects from the interfaces of the transmitter and incident bars; some of the stress pulse travels into the transmitter bar. Strain gages are located on the incident bar and on the transmitter bar. A strain versus time history is recorded from these gages. This information is used to build the flow stress curve for the specimen during loading. The equations used in the rebuilding of a stress-strain curve are:

$$\epsilon = -\frac{2c_0}{L}\int_0^t \epsilon_{reflected}\,dt \qquad (5)$$

$$\sigma = E\,\frac{A_{bar}}{A_{specimen}}\,\epsilon_{transmitted} \qquad (6)$$

where $c_0$ and E are the sound speed and elastic modulus, respectively, of the steel bars; L is the length of the specimen; A represents the cross-sectional area; and $\epsilon$ is the strain measured from the appropriate strain gages.

No elastic constants are deduced from the resulting curve, since the calculation of the elastic modulus is extremely sensitive to small shifts in the zero times of the reconstructed stress and reconstructed strain curves. The reason for the lack of accuracy is the existence of multiple wave reflections early in the response of the specimen due to its finite length; thus, the specimen does not give rise to a unified elastic response.

A test with confining pressure consisted of initially apply a static hydrostatic loading by simultaneously increasing the axial load and the pressure in the specimen chamber. These loads were then held constant, and a transient axial load was superimposed by firing the gas gun. Strain pulses, produced by the projectile impact in the incident and transmitter pressure bars, were recorded digitally.

An example of the strain records from the pressure bars generated during a brittle failure is given in Figure 2. This record is reduced in Figure 3, in which the separate pulses are shifted on the time axis to account for transit time in the pressure bars. After the specimen fractures, denoted by the maximum in the transmitted pulse signal, the load supported by the specimen drops to zero, and the incident pulse becomes totally reflected (as at a free end). The transmitted pulse is a measure of the compressive interface stress $\sigma_2$ at the back end of the specimen, *i.e.*,

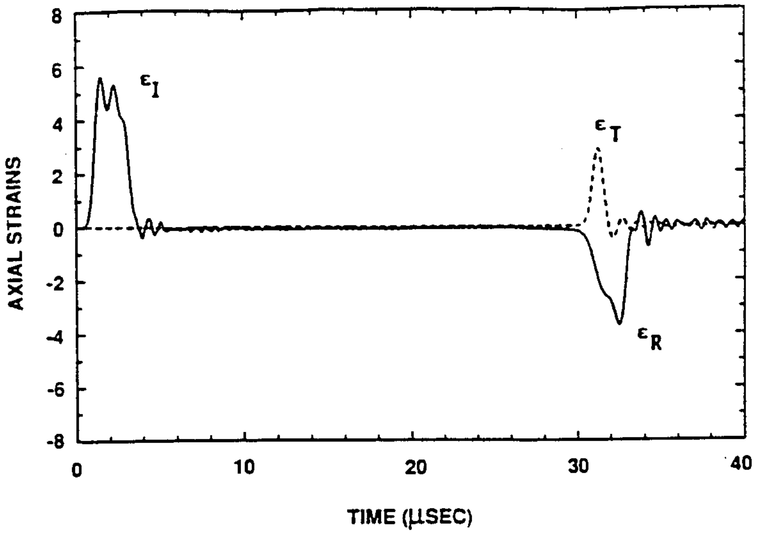

FIGURE 2. DIGITAL RECORD OF PULSES FROM HOPKINSON BAR DURING BRITTLE FAILURE.

$$\sigma_2 = E_0 \epsilon_T = \rho_T \tag{7}$$

The compressive interface stress $\sigma_1$ at the front face of the specimen is

$$\sigma_1 = E_0 (\epsilon_I + \epsilon_R) = \sigma_I + \sigma_R \tag{8}$$

where $\epsilon_I$, $\epsilon_R$, and $\epsilon_T$ are the axial compressive strain amplitudes of the incident, reflected, and transmitted pulses, and $E_0$ is the elastic modulus of the pressure bars.

It can be clearly seen from Figure 3 that the same maximum compressive stress is reached at both the front and back faces of the specimen, although there is a small time lag between the maxima. This time lag is of the order of magnitude of the wave transit time across the specimen length. The maximum stress which occurs at both faces of the specimen is considered to be the ultimate or fracture strength of the specimen. This is in fact the usual(10,11,16) interpretation of the split Hopkinson bar measurement. However, in this case, the time to fracture is very short (less than 10 μs) and it is apparent from the oscillations in the records that perfect stress equilibrium across the specimen is not achieved in this time interval.

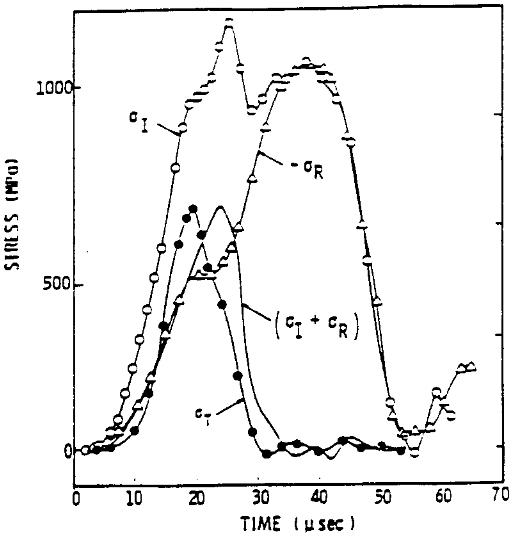

FIGURE 3. AMPLITUDE COMPARISON OF PULSES FROM PRESSURE BAR.

The average strain rate for the dynamic tests was taken as $\dot{\epsilon} = \dot{\sigma}/E$ where E is the elastic modulus and $\dot{\sigma}$ is the steepest portion of the stress versus time pulse. It is when the latter maximum strain rate regime that the specimen may be subjected to stresses in excess of the average quasi-static strength.

## EXPERIMENTAL RESULTS

As shown in Figure 4, the strength of Compglas is sensitive to confinement as well as to high strain rates, i.e., to $\dot{\epsilon} \geq 10^3 s^{-1}$. Below the latter threshold, strain rate has only a mild influence on strength. Interestingly, under relatively quasistatic loading ($\dot{\epsilon} \sim 10^{-4} s^{-1}$), an increase in hydrostatic pressure from ambient to 150 MPa raises the compressive strength (Figure 4) from 1000 to 3000 MPa; over the same pressure range at $\dot{\epsilon} = 3 \times 10^3$, the strength rises from 2600 MPa to only 3400 MPa. However, it is evident that the strengthening effect of confinement begins to saturate above $\sigma_3 = 50$ MPa. In the high strain rate region, strength is highly strain rate sensitive; plotting the data on a log-log basis indicates that $\sigma_1 - \sigma_3 \propto \dot{\epsilon}^n$, where $n = 0.67$.

The unreinforced matrix behaves in a different manner. As shown in Figure 5, strength increases with strain rate for $\dot{\epsilon} \leq 1 s^{-1}$ much more robustly than for the composite variants, but suffers a curious decline, relative to the extrapolation of this trend, for $\dot{\epsilon} \sim 3 \times 10^3$. Earlier work(17) for $\sigma_3 = 0$ suggested a mild dynamic strain rate sensitivity for this material, whereby $n \sim 0.2$. As for the composite variants, the influence of pressure appears to saturate, as evidenced in particular by the data for $\sigma_3 = 427$ MPa at $\dot{\epsilon} \sim 3 \times 10^3 s^{-1}$.

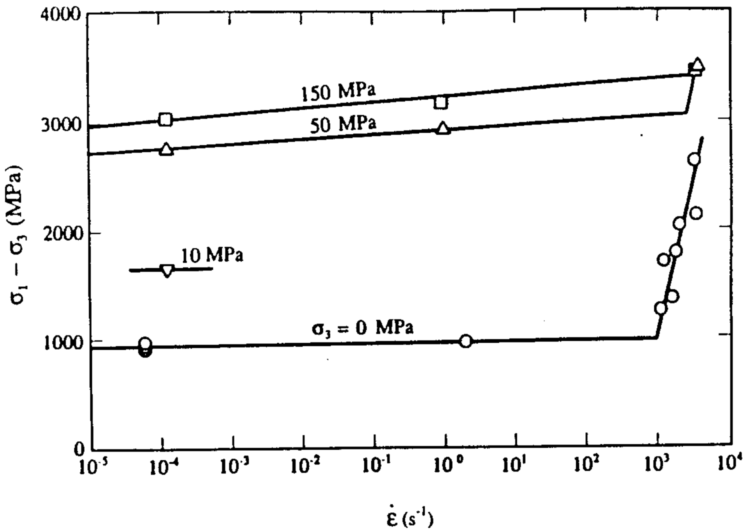

FIGURE 4. COMPRESSIVE STRENGTH VERSUS STRAIN RATE FOR 0° COMPGLAS AT VARIOUS CONFINING PRESSURES.

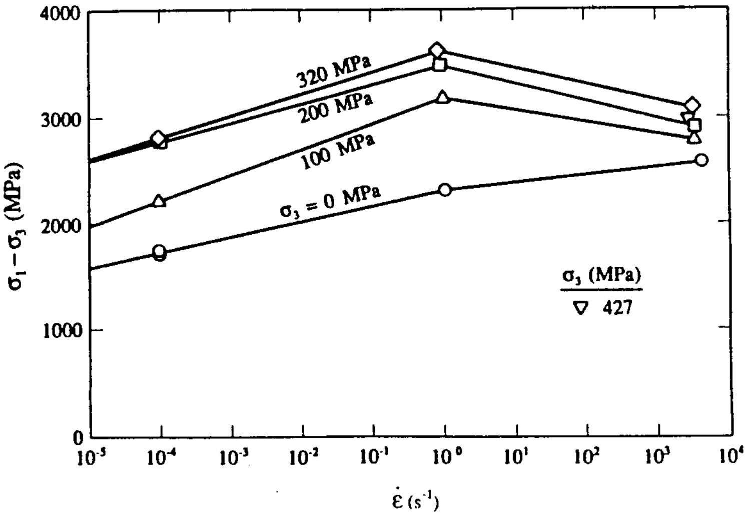

FIGURE 5. COMPRESSIVE STRENGTH VERSUS STRAIN RATE FOR UNREINFORCED CERAMIC MATRIX AT VARIOUS CONFINING PRESSURES.

Some interesting trends are revealed by considering directly the dependence of $\sigma_1 - \sigma_3$ on $\sigma_3$. For the composite material, strength initially rises rapidly with $\sigma_3$ regardless of strain rate, as shown on Figure 6. However, for $\sigma_3 \geq 50$ MPa, $\sigma_1 - \sigma_3$ is virtually constant, suggesting rapid transition from a dilatational to a pure shear failure mode. In addition, it will be noted that $\sigma_1 - \sigma_3$ rises extremely rapidly with dynamic ($\dot{\varepsilon} = 1000 s^{-1}$) loading rate at $\sigma_3 = 0$ (arrow, Figure 6). It is clear that the amplitude of this rise is greatly compressed, in terms of $\sigma_1 - \sigma_3$, at higher pressures.

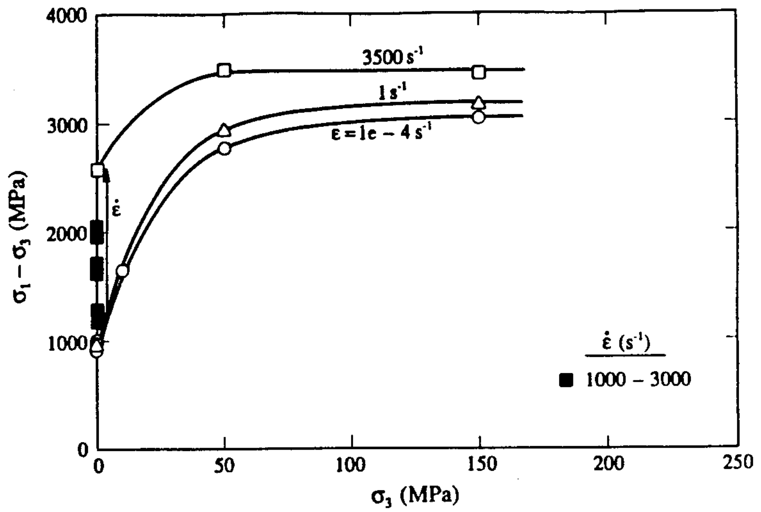

FIGURE 6. COMPRESSIVE STRENGTH VERSUS CONFINING PRESSURE FOR 0° COMPGLAS AT VARIOUS STRAIN RATES.

The unreinforced matrix material also undergoes a pressure-dependent to independent transition, as shown in Figure 7, at least for $\dot{\varepsilon} < 1000s^{-1}$. Under dynamic conditions ($\dot{\varepsilon} = 1000s^{-1}$), however, $\sigma_1$ - $\sigma_3$ versus $\sigma_3$ is virtually flat, suggesting that shear processes control failure throughout. On the other hand, the low average dynamic strength, little more than that measured at $\dot{\varepsilon} = 10^{-4}s^{-1}$, suggests that some sort of shear instability may be involved in failure at high strain rates.

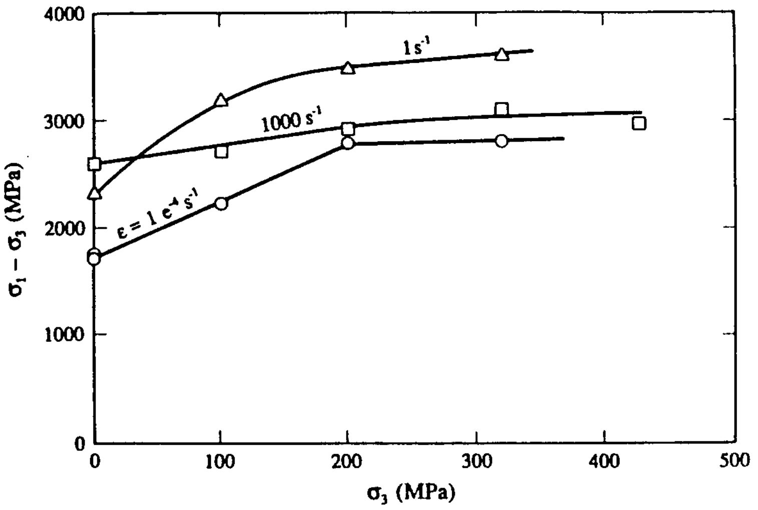

FIGURE 7. COMPRESSIVE STRENGTH VERSUS CONFINING PRESSURE FOR UNREINFORCED CERAMIC MATRIX AT VARIOUS STRAIN RATES.

## DISCUSSION

Based on Figure 4, it appears that the large pressure sensitivity manifested under quasistatic conditions for ceramic composites is severely compressed with increasing strain rate within the dynamic (SHPB) regime. This trend is reinforced in Figure 6, where $\sigma_1$ - $\sigma_3$ essentially approaches a strain rate-pressure independent limit, reached when $\sigma_3 = 50$ MPa. As observed initially, a pressure-independent differential compressive strength indicates the dominance of a shear-controlled failure process. This influence is supported by microscopic evidence, which shows that precursory and accommodating matrix microfracture in the vicinity of kinks generated under confinement at high strain rate tend to be oriented at a shear angle relative to the load axis. Earlier work(18) showed that clusters of such cracks, which are required to permit kink formation, tend to be axially oriented at low strain rates in the absence of confinement. A pressure-induced transition in matrix microcrack mode from dilatational (mode I) to shear (mode II) provides a rationale for the tendency of the composites to tend toward a pressure-independent strength asymptote at a given strain rate. Moreover, the matrix origin of the asymptote is reflected in similar trends observed for the matrix itself (Figure 7). The fact that composite strain rate strengthening is not additive to pressure hardening appears to be a consequence of the peculiar loss of matrix strength under confinement at high rates of loading (Figure 5). Similar behavior has been observed for $Al_2O_3$ and duplex $Al_2O_3 \cdot B_4C$.(19) Since failure is so rapid and catastrophic, it has proven impossible to date to "capture" the early stages of damage development at high strain rate for microscopic analysis. However, it nevertheless is possible to offer a rational explanation based on crack kinetics and ensemble stability considerations.

It is known(7) that at low strain rates and zero confining pressure, failure in monolithic ceramics occurs by the gradual nucleation of a large population of microcracks. At some characteristic stress level, these interact with one another, coalesce, and reduce the specimen to a pile of fine-scale dust. For higher (SHPB) strain rates, still under zero confining pressure, crack kinetics effects (i.e., crack inertia) delay failure to higher stress levels, and as a consequence a much higher population of microcracks is predicted.(8,9) If true, such a population would necessarily correspond to a finer fragment size distribution upon failure; this recently has been shown(20) to be precisely the case for SiC.

At low strain rates, microcracks nucleate more-or-less homogeneously within the specimen, with the role of the confining pressure being the stabilization of the microcrack assemble. This stabilization is reflected in the pressure-dependent hardening evidenced (Figure 11) at strain rates of $1s^{-1}$ and $10^{-4}s^{-1}$. Eventually, however, the cracks, probably having grown somewhat, interact with one another to form a macroscopic fault, and the specimen fails.

Compressive failure at high strain rates under confinement can only be explained by extrapolating from the preceding observations as follows. Regardless of the state of confinement, crack kinetics are always a factor. Thus, under zero confining pressure, failure is a result of the normal component of the local stress field acting on the crack system. This causes the specimen to fail throughout its volume by exploding into fragments characterized by a fairly tight size distribution. Once confining pressure is applied, however, and the local crack opening load is counteracted, this mode of failure is prohibited. Failure then occurs by the formation of a shear fault via the coalescence of en echelon microcracks. Since these microcracks form homogeneously under dynamic loading, there are more of them, but they are smaller in size than those within the corresponding ensemble present in specimens loaded at lower strain rates. The latter have time to grow, forming inhomogeneously at lower applied stress levels near local stress concentrations. It has been shown by Broek and Bombolakis(21) that small cracks arranged en echelon grow into faults at a significantly lower applied compressive stress than that required to enlarge an equivalent (total length of en echelon array) large crack.

The results shown in Figure 5 are consistent with this hypothesis. At low (near zero) confining pressures, the strength for $\dot{\varepsilon} > 1000s^{-1}$ exceeds that for lower strain rates. This is so because failure in this pressure regime is dominated by the coalescence of microcracks, whose nucleation and growth kinetics permit the achievement of higher stress levels prior to failure. However, with increasing confining pressure, the ensemble of dynamic microcracks is less stable in shear than that generated at lower strain rates, and so the dynamic failure strength quickly drops below the characteristic of quasistatic conditions.

Returning to consideration of Compglas composites, it is possible to apply the preceding argument to explain the marked diminution in the high strain rate pressure-induced strength differential versus that at low strain rates.

As noted earlier, kink formation can only occur by means of matrix microfracture accommodation, which corresponds under rapid loading at high confinement to ensembles of shear microcracks. These local prekink zones degenerate unstably into shear microfaults according to the same kinetics that control the failure of bulk samples of monolithic matrix, and reduce the overall strength level accordingly.

## ACKNOWLEDGEMENT

The support of the Office of Naval Research under Contract No. N00014-92-C-0093 is gratefully acknowledged.

## REFERENCES

1. Cheatham, J. B., 1968, Mechanical Behavior of Materials Under Dynamic Loads, p. 388.
2. Heard, H. C., 1960, Rock Deformation, p. 193
3. Lindholm, U. S., Yeakley, L. M., and Nagy, A., 1974, *Int. J. Rock Mech. Min. Sci.*, Vol. 11, p. 181.
4. Serdengecti, S. and Boozer, G. D., 1961, "The Effects of Strain Rate and Temperature on the Behavior of Rocks Subjected to Triaxial Compression," *Proc. 4th Symp. Rock Mech.*, Pennsylvania State University, p. 83.
5. Wilkins, M. L., 1978, *International Journal of Engineering Science*, Vol. 16, p. 793.
6. Arrowood, R. and Lankford, J., 1987, *J. Mat. Sci.*, Vol. 22, p. 3737.
7. Lankford, J., 1983, *Fract. Mech. of Ceram.*, Vol. 5, p. 652.
8. Grady, D., E., 1982, *J. of Applied Phys.*, Vol. 53, p. 322.
9. Grady, D. E. and Hollenbach, R. E., 1977, "Rate-Controlling Processes in the Brittle Failure of Rock," Sandia Report SAND 76-0659, Sandia National Laboratory, Albuquerque, NM.
10. Green, S. J. and Perkins, R. D., 1968, *Proc. Tenth Symp. on Rock Mechanics.*
11. Perkins, R. D., Green, S. J., and Friedman, M., 1970, *Int. J. Rock Mech. Min. Sci.*, Vol. 7, p. 527.
12. Lankford, J., 1991, "Compressive Damage and Failure at high Loading Rates in Graphite Fiber-Reinforced Polymeric Matrix Composites," *Ceramic Transactions*, Vol. 19, Advanced Composite Materials, ed., M. D. Sacks, The American Ceramic Society, Westerville, OH, p. 553.
13. Lankford, J., (in press), "Micromechanisms of Compression Failure in a Glass Fiber-Reinforced Amorphous Thermoplastic," *J. of Mat. Sci.*
14. Christensen, R. J., Swanson, S. R., and Brown, W. S., 1972, *Experimental Mechanics*, Vol. 12, p. 508.
15. Lindholm, U. S. and Yeakley, L. M., 1968, *J. of Exper. Mech.*, Vol. 8, p. 1.
16. Kumar, A., 1968, *Geophysics*, Vol. 33, p. 501.
17. Lankford, J., 1988, *Ceramic Engineering and Science Proceedings*, Vol. 9, p. 843.

18. Lankford, J., 1985, "Compressive Strength and Damage Mechanisms in a SiC-Fiber Reinforced Glass-Ceramic Matrix Composite," *Proc. Fifth Int. Conf. on Comp. Mat.*, eds., W. C. Harrigan, J. Strife, A. K. Dhingra, TMS AIME, New York, p. 587.

19. Johnson, G. R., Holinquist, T. J., Lankford, J., Anderson, C. E., and Walker, J., 1990, "A Computational Constitutive Model and Test Data for Ceramics Subjected to Large Strains, High Strain Rates, and High Pressures," DARPA Technical Report, Contract No. DE-AC04-87Al-42550.

20. Lankford, J. and Blanchard, C. R., 1991, *J. Mat. Sci.*, Vol. 26, p. 3067.

21. Brace, W. F. and Bombolakis, E. G., 1963, *J. of Geophys. Res.*, Vol. 68, p. 3709.

*Journal of Materials Science (in press)*

# III.

# FAILURE OF FIBER-REINFORCED CERAMIC MATRIX COMPOSITES UNDER DYNAMIC LOADING CONDITIONS

By
James Lankford
Southwest Research Institute
San Antonio, Texas 78228-0510

## ABSTRACT

High-strain rate compressive failure mechanisms in fiber-reinforced ceramic matrix composite materials have been characterized. These are contrasted with composite damage development at low-strain rates, and with the dynamic failure of monolithic ceramics. It is shown that it is possible to derive major strain-rate strengthening benefits if a major fraction of the fiber reinforcement is aligned with the load axis. This effect considerably exceeds the inertial microfracture strengthening observed in monolithic ceramics and non-aligned composites. Its basis is shown to be the trans-specimen propagation time period for heterogeneously-nucleated, high-strain kink bands. For high strain-rate tensile loading conditions, it is found that behavior is not correctly described by the current matrix fracture/fiber pullout models. This is a consequence of the rapid and extreme frictional heating produced at the fiber-matrix interface by sliding velocities on the order of 100 m/s. At rapid loading rates, the near-interface matrix appears to virtually melt, and the frictional interface shear resistance is reduced to the point that the fibers debond throughout the specimen, and pull out without failing. This suggests that for sufficiently rapid loading, the stress to fail the composite will approach that merely to create the initial matrix crack, i.e., a stress level well below the ultimate strength normally attainable under quasi-static conditions.

# INTRODUCTION

One of the major developments in the effort to enhance the ability of brittle materials to serve in structural applications has been their reinforcement with continuous ceramic fibers. Extensive research has shown that this can provide improved strength, toughness, and "ductility," principally through mechanisms involving matrix microfracture and frictional, energy-absorbing fiber pullout. However, most of the developmental work has been performed at virtually quasistatic rates of tensile loading. Many structural applications, on the other hand, require resistance to dynamic loads produced under more complex loading conditions. During flexural loading of fiber-reinforced ceramics, for example, it is often observed that failure of the specimen will initiate on the compressive side, at local stresses well below the needed to cause tensile-mode damage. The work discussed in the following has been aimed at exploring the response of fiber reinforced ceramics to dynamic, as well as quasistatic, compressive and tensile loading.

# BACKGROUND

## Compressive Behavior

It is by now well known that brittle materials subjected to high rates of compressive loading often exhibit strengths much greater than those characteristic of slow or quasistatic rates.[1-5] The degree of strengthening observed is generally too high, or too strain-rate sensitive, to be explained on the basis of the suppression of thermally activated crack tip processes, although the latter does impart a mild rate-dependent strength benefit.[1] For example, the author has shown that for strain rates $\geq 10^3$ $s^{-1}$, obtainable within the split Hopkinson pressure bar (SHPB), the compressive strength of certain classes of monolithic ceramics follows a cube-root dependence upon strain rate. Others have obtained similar results for rocks, in both compression and tension.[2-7]

In fact, it has been shown by Grady and Lipkin[8] that analyses based on a variety of physical criteria (work of fracture, least action law, inertia of flaws to crack initiation) likewise all lead inevitably to a cube-root tensile fracture relationship between strength and strain rate. Since brittle compressive failure is known to correspond to the coalescence of a multitude of microscopic cracks nucleated within local tensile regions, it is therefore not surprising that equivalent failure dynamics should obtain for both tension and compression. Generalizing the situation, Grady and Kipp observe[3] that such results suggest that a cube-root strain-rate dependence represents the upper limit that can be obtained in the dynamic brittle failure process. This probably is true for monolithic materials, but it will been seen that the microstructures of ceramic matrix composites can be manipulated to yield a much higher degree of strain-rate sensitivity.

## Tensile Behavior

Although ceramic matrix composites reinforced with silicon carbide fibers currently are candidates for a variety of applications in which their nominal material and mechanical properties appear to be extremely desirable, their response to truly dynamic, or impulsive, tensile loading has not yet been explored either theoretically or experimentally. This is not to say that the effect of loading rate, *per se*, on fiber-matrix interaction has not received study; in fact, it has. Goettler and Faber,[9] for example, have shown that the interfacial shear strength within the SiC fiber-borosilicate glass system increases with stress rate. On the other hand, Philips[10] has observed that both the work of fracture and fiber pullout length are constant with increasing rate of loading for carbon fiber-reinforced LAS pyroceram. However, it should be noted that the fiber sliding rates in these experiments were low, on the order of $10^{-7}$ to $10^{-4}$ m/s. Under the rapid loading conditions envisioned here, fiber sliding rates may attain velocities as high as 100 m/s.

The mechanisms responsible for the excellent quasi-static strength, deformation, and toughness of fiber-reinforced ceramics have been thoroughly reviewed by Evans and Marshall.[11] Basically, "good" fiber-reinforced ceramics exhibit tensile stress-strain behavior as shown schematically in Figure 1. The initial deviation from linearity corresponds to the formation of the first crack in the matrix, which extends entirely across the specimens, breaking very few fibers en route. With increased loading, other matrix cracks are initiated, separated by a spacing characteristic of the frictional stress transfer afforded by the fiber-matrix interface. Further non-linear deformation is produced by unbroken fibers sliding within these crack-created "blocks" of matrix material. Once the specimen gage section is full of cross-sectional matrix cracks, the surviving fiber bundles begin to fail, i.e., the ultimate strength ($\sigma_U$) has been attained.

The specific parameter that determines the rate of load transfer from the fibers to the matrix, and thus the ultimate strength of the composite, is simply the frictional resistance to fiber "pullout." For micromechanics purposes, it is convenient to treat the latter as an effective shear stress, $\tau$, characteristic for a debonded interface. However, from a materials response viewpoint, it is more relevant[3] to view $\tau$ (to a first order) as $\mu q_N$, where $\mu$ is a classic friction coefficient, and $q_N$ is the residual stress normal to the interface. Thus, the question at issue reduces to the effect of dynamic loading upon $\mu$ and $q_N$.

Study of sliding friction between ceramic couples indicates that $\mu$ generally increases with sliding velocity; such behavior is primarily a consequence of the interfacial temperature rise associated with rapid sliding. Under steady state sliding conditions, the local temperature may rise hundreds of degrees,[12] promoting local plasticity and thermal expansion. For the case of fibers sliding within a confined space, thermally-induced dimensional changes would tend to alter $q_N$, while the softening of interface constituents, permitting frictional energy-absorbing plasticity, would be reflected in $\mu$. In this regard, it is relevant to note that for LAS pyroceram couples sliding under ambient conditions, an increasing in the sliding velocity from 0.5 m/s to 1.8 m/s doubled the friction coefficient.[12] After 500s of sliding at each velocity, corresponding near-interfacial temperatures were 110° and 450°C, respectively. Moreover, measurements of fiber displacement caused by quasi-static microhardness indentation indicate[13] that for strong, tough SiC fiber-reinforced pyroceram, the fiber/matrix friction coefficient may be as low as 0.01; under these circumstances, i.e., low sliding velocity, frictional temperature increases are negligible. However, in light of the apparent small amplitude of $\mu$, combined with its major role in the composition failure process, it is clear that changes induced in it by dynamic loading could have a profound effect on both strength and (effective) ductility.

## OBJECTIVE

The objective of the present work is to review the effect of high strain rates upon compressive and tensile failure processes in a representative fiber-reinforced ceramic matrix composite. It will be shown that tensile failure ultimately must be interpreted in terms of intense thermal effects at the fiber/matrix interface, while compressive failure is controlled by the kinetics of kink band nucleation and propagation.

## EXPERIMENTAL APPROACH

### Material

The composite chosen for study was fabricated* by United Technologies (UTRC), and has been characterized microstructurally by Brennan.[14] Briefly, the panel from which the specimens were extracted was laid up using 46 v/o Nicalon silicon carbide fibers; the latter are approximately 16 μm in diameter. The matrix was the UTRC lithium-aluminosilicate glass ceramic designated as LAS-II, which is essentially Corning 9608 pyroceram modified by replacing 3 w/o $TiO_2$ with 3 w/o $ZrO_2$, and adding 5 w/o $Nb_2O_5$. The heat-treated matrix consists of grains ranging in size from ~ 0.5 to 2.0, crystallized in the β-quartz-silica solid solution LAS phase. In addition, the fibers themselves are altered by the processing, their outer layer consisting of a 200-400 Å thick ring of almost pure carbon. This carbon-rich zone is weakly bonded to both the matrix and the fiber, and is thought[13] to be responsible for the low value of the quasi-static fiber-matrix sliding friction coefficient.

Two basic composite systems were studied. In the first (0° variant), the fibers were oriented unidirectionally, and compression specimen axes were aligned with the fibers. For the second variant, fibers were laid up in 200 μm thick planar bundles, with the fibers in alternating layers at 90° to one another. Specimen axes in this case were either parallel to one set of fibers (0/90), or lay at 45° to both sets (45/45). The matrix itself also was tested.

---

* Compglas®, United Technologies Research Center.

### Testing Procedures

Testing was performed using standard hydraulic test machines for strain rates in the range of $10^{-4}$ $s^{-1}$, as well as the SHPB, which produced dynamic strain rates on the order of 350 $s^{-1}$ to 1500 $s^{-1}$. Techniques specific to compressive and tensile pressure bar testing are described in detail elsewhere.[15,16]

## RESULTS

As shown in Figure 2, the compressive strength of the composite material is relatively strain-rate independent for $\epsilon \leq 10^2$ $s^{-1}$, above which the compressive strengths of 0° and 0/90 variants is proportional to $\dot{\epsilon}^{0.77}$, while for the 45/45 material, strength is proportional to the cube-root of the strain rate. It should be observed that the relative strength ordering at low strain rates is preserved within the high-rate regime, and that the strength decrement between 0° and 0/90 variants is essentially constant.

For the matrix material alone, $\sigma_c$ versus $\dot{\epsilon}$ is basically constant until $\dot{\epsilon} \approx 10^3$ $s^{-1}$, above which the cube-root relationship again holds. Within this strain rate regime, pyroceram failure is catastrophic, and brought about by the rapid coalescence of a multitude of microcracks.

It has been shown elsewhere[17] that at low-strain rates, the composite material fails in compression by axial matrix microfracture, producing macroscopic "columns;" these fail by a general multi-fiber buckling process. This is not what happens at high-loading rates. Study of damaged, but unfailed, 0° and 0/90 SHPB specimens reveals no buckling, but instead (Figure 6) a number of isolated, but macroscopic, shear bands. At least one end (usually both ends) of each such band is associated with a vertical microfracture zone (arrow, Figure 3); the latter appears to accommodate the intense shear within a given band. Behavior of the 45/45 composite differed in that it simply disintegrated catastrophically, similar to the matrix material itself.

Comparing d and $l_o$ in Figure 4, it is evident that kink band shear strains ($d/l_o$) can easily exceed unity. These are accomplished by the propagation of kinks in SiC fibers (Figure 5), accompanied by local matrix microfracture.

## Tension

Tensile deformation behavior is summarized in Figure 6. Almost hidden in the initial rise of the high strain rate curves lies the complete quasi-static stress-strain response; in all the SHPB experiments, the ultimate strength is significantly higher than the quasi-static value. At the two highest strain rates, however, the strain at failure is drastically reduced versus that which obtains at $\dot{\epsilon} = 346\ s^{-1}$, and there is no obvious yield point. Failure at the latter rate is followed by an extensive regime of continuously declining strength, while in the higher rate dynamic experiments, the post-failure region consists of a series of minor stress-strain peaks of declining amplitude.

Optical examination revealed within the latter failed specimens periodic matrix microcrack ensembles previously identified as characteristics of, if not required for, non-catastrophic composite failure. Crack spacing data is summarized in Table I, where D is the saturation crack spacing. It should be noted that similar multiple microcracks could not be discerned for specimens tested at the two highest dynamic strain rates, for which D must be equal to or greater than the specimen gage length.

Table I. Crack Spacing Measurements

| $\dot{\epsilon}$ ($s^{-1}$) | D (µm) |
|---|---|
| $1.15 \times 10^{-5}$ | 310 ± 32 |
| 346 | 515 ± 43 |
| 947 | ≥ 4445 (gage length) |
| 1100 | ≥ 4445 (gage length) |

Fiber pullout was strikingly strain rate dependent , as shown in Figure 7. Under quasi-static conditions (A), the pullout length varied a great deal. As the loading transits to the dynamic regime (B), this variation is reduced, and so is the average pullout length; further reduction in pullout is observed at a still higher strain rate (C). Finally, at the highest strain rate (D), a major change in behavior occurs, i.e., a large number of fibers are pulled out intact, as evidenced by the horizontal coincidence of their originally ground (parallel) ends.

In addition to these macroscopic features, the effect of strain rate on fracture mode is manifest at the microscopic level as well. This is demonstrated in dramatic fashion in Figure 8, where (B) and (D) are typical of the appearance of all the SHPB specimens. At slow rates (A), fibers pull out cleanly, and at high magnification, the fracture surface has a simple cleavage appearance. On the other hand, under dynamic loading (B), fibers are pulled out attended by globular debris; close inspection (D) shows that the latter appears to have solidified from a liquid state. The uppermost particle, in fact, is barely attached by a neck apparently solidified just prior to droplet separation.

## DISCUSSION

### Compression

The fact that the strengths of the monolithic matrix and the 45/45 composite increase as $\dot{\epsilon}^{-0.3}$ at high-loading rates, and that both fail via rapid microcrack coalescence, suggests that inertia-controlled, homogeneous microfracture is responsible for failure. This also suggests that the presence of fibers at other than 0° provides a weakening effect which probably derives from their role as "microanvils," fracturing the matrix at a significantly lower stress than that which obtains in the pure matrix. The presence of such effective crack initiators in 0/90 material evidently accounts for the persistent difference in strength between 0° and 0/90 composites over the entire strain-rate regime. Further, since the difference exists at high loading rates, tensile microfracture inertia must be included within the observed strain-rate sensitivity for both 0° and 0/90 layups. However, the high strain rate specimens actually fail by shear fault nucleation and propagation; the latter can be shown to contribute an additional, significant rate-dependent term.

In particular, the maximum propagation velocity possible for such a fault is limited by the shear wave speed in the composite. By taking this into account, it can be shown[15] that the dynamic compressive strength of a 0°-reinforced composite containing a preexisting kink band should be proportional to the strain rate to the first power. However, it should be appreciated that this process actually cannot take place without local accommodation of the initial 0°-kink responsible for shear band formation. Evans and Adler,[18] for example, have analyzed the micromechanics of kinking in three-dimensional composites capable of at least some plastic flow. Consideration of their result, which includes a variety of microstructural and material parameters, indicates that the compressive strength depends mainly on the matrix yield strength. In the present instance, the matrix clearly does not yield, but can fragment via local tensile microfracture, and thereby produce a shear instability capable of accommodating a kink by the sliding/rotation of the fragments.

Such accommodations appear to be responsible for the off-fault plane microfracture attending the ends of the present kink bands (Figure 3). Since the kink cannot form until the matrix "yields," it is likely that local tensile microfracture precedes dynamic kink formation. This in accord with the earlier suggestions that a differing microfracture threshold is responsible for the observed constant (strain rate-independent) difference between 0° and 0/90 compressive strengths.

Accommodation by local microfracture would imply, of course, a cube root strain-rate contribution to the composite dynamic compressive strength, in addition to the first power factor derived for kink propagation. This apparently is reflected in the experimentally-derived strain rate exponent of 0.77.

## Tension

It is apparent that under quasi-static conditions, the composite behaves in the standard way. The observed stress-strain curve is similar to that reported[19] for identical material tested in a different tensile configuration, and the matrix microcrack spacings (310 μm) are in excellent agreement with those (290 μm) reported[5] for a similar Nicalon-LAS system. Based on the wide distribution in fiber pullout length (Figure 7A), it is reasonable to assume that the equilibrium nature of the test provided ample opportunity for the stress distribution within the microcracked matrix to sample the statistical flaw distribution within the fiber bundle.

However, the crack spacing is significantly greater (515 μm) at the lowest dynamic loading rate, and apparently is equal to the specimen gage length (at least) for still higher rates. The significance of an increasing crack spacing can be explored by appealing to theoretical treatment[20] of composite strength as controlled by matrix microfracture and fiber pullout, which in turn is governed by crack spacing, the fiber-matrix sliding friction coefficient, and the Weibull flaw distribution within the SiC fibers.[19]

Based on this concept, it is possible to compute from the measured crack spacings and appropriate material properties the apparent values of the fiber sliding shear stress, $\tau$, and the associated ultimate strength. These are summarized in Table II.

Table II. Theoretical and Experimental Fracture Parameters

| $\dot{\epsilon}$ ($s^{-1}$) | $\tau$(MPa) | $\sigma_U^{Th}$ (MPa) | $\sigma_U^{Exp}$ (MPa) |
|---|---|---|---|
| $1.15 \times 10^{-5}$ | 2.2 | 433 | 585 |
| 346 | 1.02 | 429 | 683 |
| 947 | 0.038 | 420 | 868 |
| 1100 | 0.038 | 420 | 810 |

It is obvious that the theoretical model[20] is inconsistent with the physical events attending failure at higher strain rates. In particular, following nucleation of the dominant matrix crack, fibers begin to slide at such a rate that $\tau$ drops precipitously. Values of $\tau$ as low as 0.038 MPa, combined with the observation of globular debris associated with fiber pullout, suggest that the matrix is melting during fiber sliding. This is not as unreasonable as it might seem, given the apparent velocities involved in the pullout process. For the highest strain rate, 1100 $s^{-1}$, fibers extracted over a distance of approximately 4.5 mm in about 2 μs. This corresponds to a sliding speed of 2250 m/s, a rate which would probably produce immense frictional heating, even in so short a time.

It is interesting to consider the strength-strain rate dependence for the three dynamic experiments, plotted in Figure 9. Once the strain rate exceeds some critical value, situated between 346 $s^{-1}$ and 947 $s^{-1}$, the specimen contains only one major crack. The faces of this crack are bridged by fibers sliding with little resistance within the matrix. Because $\tau$ is so low, frictional load transfer is insufficient to load the sliding fibers to the level necessary to sample their Weibull flaw distribution. Only those fiber segments bridging, and extending a short distance below, the main crack interface experience high stresses, and these segments are short – so short that the fibers must fail at sites other than their weakest links.

Thus, at $\dot{\epsilon} = 947\ s^{-1}$, fibers are sliding throughout the specimen when the stress level near the interface reaches a level sufficient to break a number of the fibers within the sector. The overall stress level drops, as the load is transferred to the remaining "stronger" fibers, causing the load to increase again (the first post-failure peak in Figure 6), a process which is repeated several times until all the fibers have failed in the near-interface region of the main crack. On the other hand, at $\dot{\epsilon} = 1100\ s^{-1}$, the sliding shear resistance is sufficiently low that just below the stress level required to fail the most highly stressed fibers, they break free all along the specimen length, creating the first load drop (failure), following which subsequent load transfer and near-interface fiber fracture proceed as described above.

The crucial implication of this scenario is that at still higher strain rates, the ultimate strength will be even further reduced. Eventually, the strength will approach that required simply to create the first matrix crack.

## CONCLUSIONS

Dynamic loading conditions introduce factors that have not previously been appreciated into the failure mechanics and strength criteria for fiber-reinforced ceramics. Under rapid compressive loading, the kink band mechanism contributes to a marked strengthening with rising strain rate. The result of high strain rate tensile loading, however, is ultimately deleterious to composite strength. Fiber sliding, normally the basis for tensile strengthening and toughening relative to the unreinforced ceramic matrix, occurring at a high velocity leads to matrix melting and a virtually total loss of shear strength. These findings clearly support the conclusion that the extrapolation of failure theories based upon equilibrium, quasistatic boundary conditions may be totally unfounded for complex material systems based on composite technology.

## ACKNOWLEDGEMENT

The support of the Office of Naval Research through Contract No. N00014-92-C is gratefully acknowledged.

## REFERENCES

1. J. Lankford, "The Role of Subcritical Tensile Microfracture Processes in Compression," *Fracture Mechanics of Ceramics*, 5 (1983) pp. 625-637.

2. D. E. Grady and R. E. Hollenback, "Rate-Controlling Processes in the Brittle Fracture of Rock," *Geophys. Res. Letters*, 6 (1979) pp. 76.

3. D. E. Grady and M. E. Kipp, "The Micromechanics of Implant Fracture of Rock," *Int. J. Rock Mech. Min. Sci.*, in press (1979) pp. 293-302.

4. S. J. Green and R. D. Perkins, "The Role of Subcritical Tensile Microfracture Processes in Compression Failure of Ceramics," K. E. Gray (ed.), *Proceedings of 10th Symposium on Rock Mechanics*, American Institute of Mining, Metallurgical, and Petroleum Engineers, Austin, TX (1968) pp. 35-54.

5. J. Lankford, "Inertia as a Factor in the Dynamic Strength of Brittle Materials," *J. Am. Cer. Soc.*, 65 (18) (1982) C-112.

6. D. L. Birkimer, "A Possible Failure Criterion for the Dynamic Tensile Strength of Rock," K. E. Gray (ed)., *Proceedings of 12th Symposium on Rock Mechanics*, American Institute of Minning Metallurgical, and Petroleum Engineers, Austin, TX (1971) pp. 573-584.

7. M. J. Forrestal, D. E. Grady, and K. W. Schuler, "An Experimental Method to Estimate the Dynamic Fracture Strength of Oil Shale in the $10^3$ to $10^4$ $s^{-1}$ Strain Rate Regime," *Int. J. Rock Mech. Min. Sci.* 15 (1978) pp. 263-265.

8. D. E. Grady and J. Lipkin, "Criteria for Impulsive Rock Fracture," *Geophys. Res. Letters*, 7 (1980) pp. 255.

9. R. W. Goettler and K. T. Faber, "Interfacial Shear Stresses in Fiber-Reinforced Glasses," 37 (1989) pp. 129-147.

10. D. C. Phillips, "Interfacial Bonding and the Toughness of Carbon Fibre Reinforced Glass and Glass-Ceramics," *J. Mater. Sci.*, 9 (11) (1974) pp. 1847-1854.

11. A. G. Evans and D. B. Marshall, "The Mechanical Behavior of Ceramic Matrix Composites," *Acta Metall.*, 37 (10) (1989) pp. 2567-2583.

12. D. C. Cranmer, "Tribological Properties of Glass Ceramics," *Com. Am. Ceram. Soc.*, 67 (9) (1984) C-180-82.

13. D. B. Marshall, *Interfaces in Ceramic Fiber Composites,* eds. J. A. Pask and A. G. Evan (Plenum Press, New York, 1988) pp. 859-868.

14. J. J. Brennan, "Additional Studies of SiC Fiber Reinforced Glass-Ceramic Matrix Composites" (ONR Annual Report, Contract No. N00014-82-C-0096, 1984).

15. J. Lankford, "Dynamic Compressive Fracture in Fiber-Reinforced Ceramic Matrix Composites," *Materials Science and Engineering*, A107 (1989) pp. 261-268.

16. J. Lankford, H. Couque, and A. Nicholls, "Effect of Dynamic Loading on Tensile Strength and Failure Mechanisms in a SiC Fiber-Reinforced Ceramic Matrix Composite," *J. Mat. Sci.*, 27 (1992) pp. 930-936.

17. J. Lankford, "Compressive Strength and Damage Mechanisms in a SiC-Fiber Reinforced Glass-Ceramic Matrix Composite," W. C. Harrigan, J. Strife, and A. K. Dhingra (eds.), *Proceedings of the 5th International Conference on Composite Materials (ICCMV)*, (TMS-AIME, Warrendale, 1985) pp. 587-602.

18. A. G. Evans and W. F. Adler, *Acta Met.*, 26 (1978) pp. 725.

19. K. M. Prevo, "Advanced Characterization of SiC Fiber Reinforced Glass-Ceramic Matrix Composites," (ONR Interim Report, Contract No. N00014-81-C-0571, 1983).

20. H. C. Cao, E. Bischoff, O. Sbaizero, M. Ruhle, and A. G. Evans, "Effect of Interfaces on the Properties of Fiber-Reinforced Ceramics," *J. Am. Cer. Soc.*, 73 (6) (1990) pp. 1691-1699.

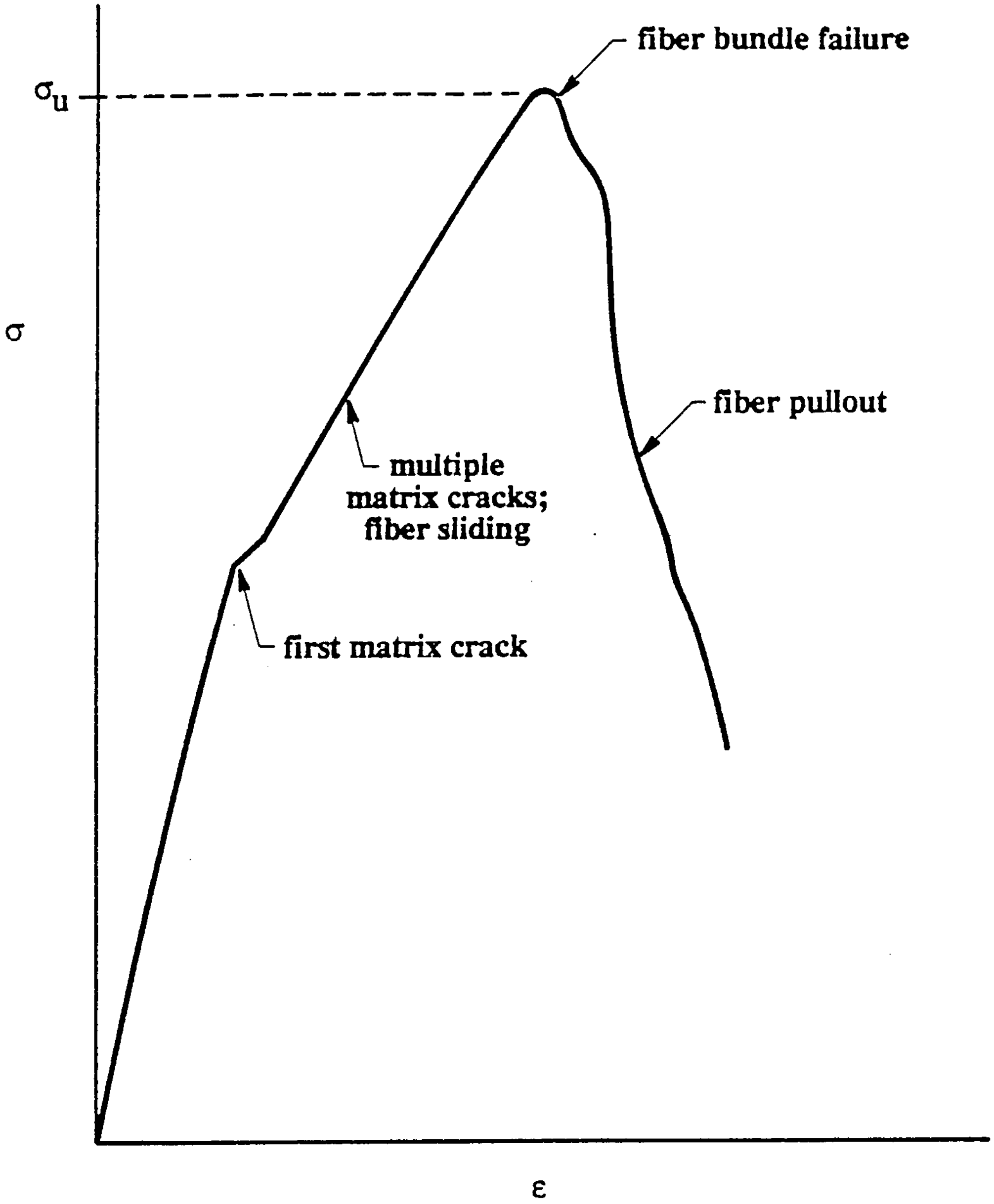

Figure 1. Schematic of fiber-reinforced composite stress-strain response and associated damage processes.

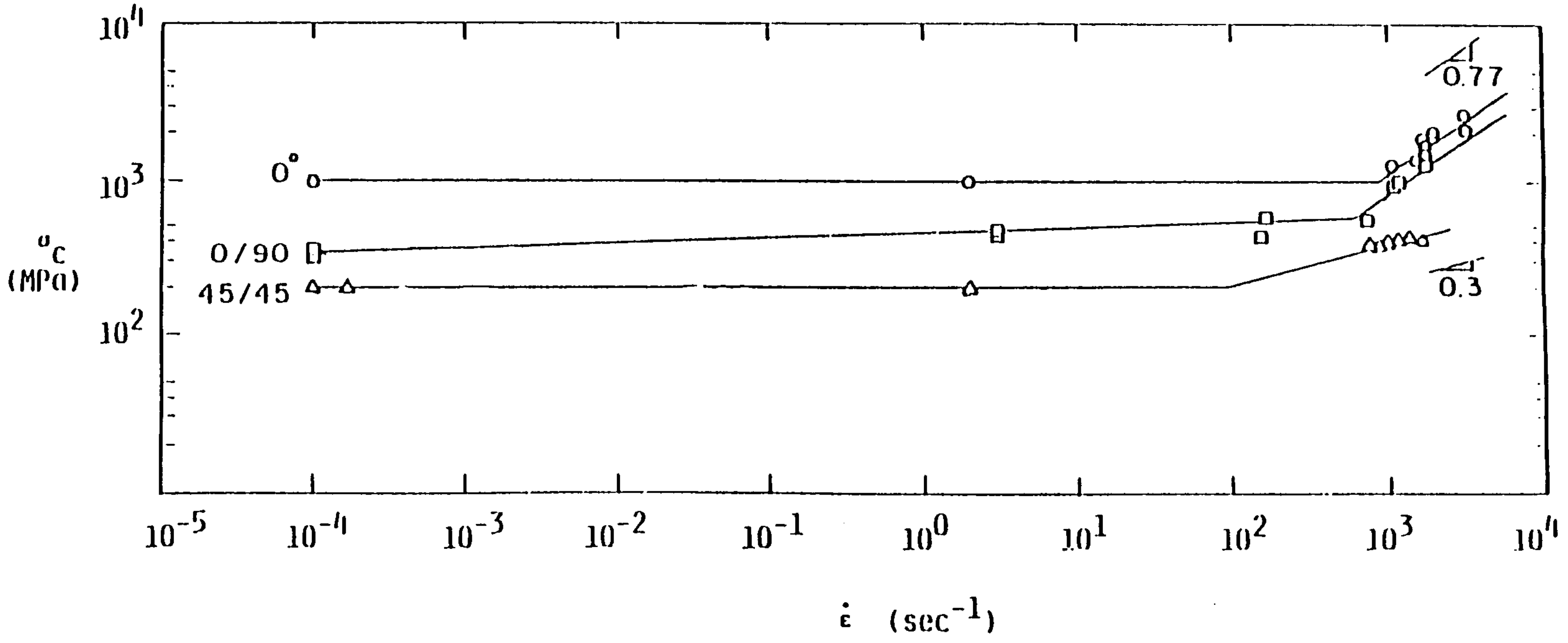

Figure 2. Compressive strength versus strain rate for SiC fiber-reinforced pyroceram.

Figure 3. Kink band crossing several 0/90 plies; stress axis vertical, $\dot{\epsilon} \simeq 2 \times 10^3\ s^{-1}$. Arrow indicates zone of microfracture within 90° ply at end of band.

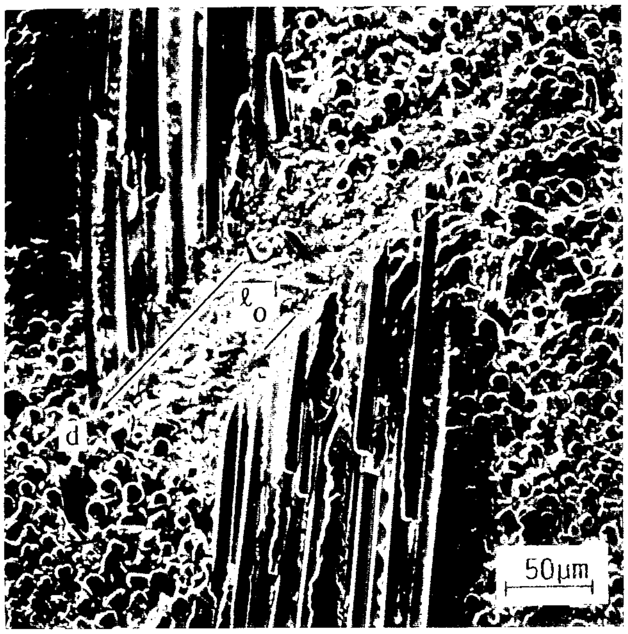

Figure 4. Kink band in 0/90 composite, showing shear displacement d versus shear gage length $l_o$; $\dot{\epsilon} = 10^3$ $s^{-1}$, stress axis vertical.

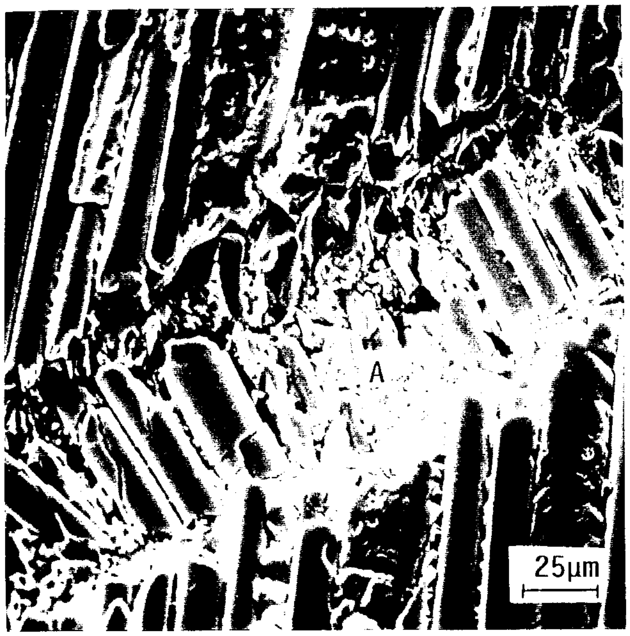

Figure 5. Kink band in 0/90 composite, showing microfragmentation of matrix to accommodate SiC fiber fracture and rotation; $\dot{\epsilon} = 2 \times 10^3\ s^{-1}$, stress axis vertical.

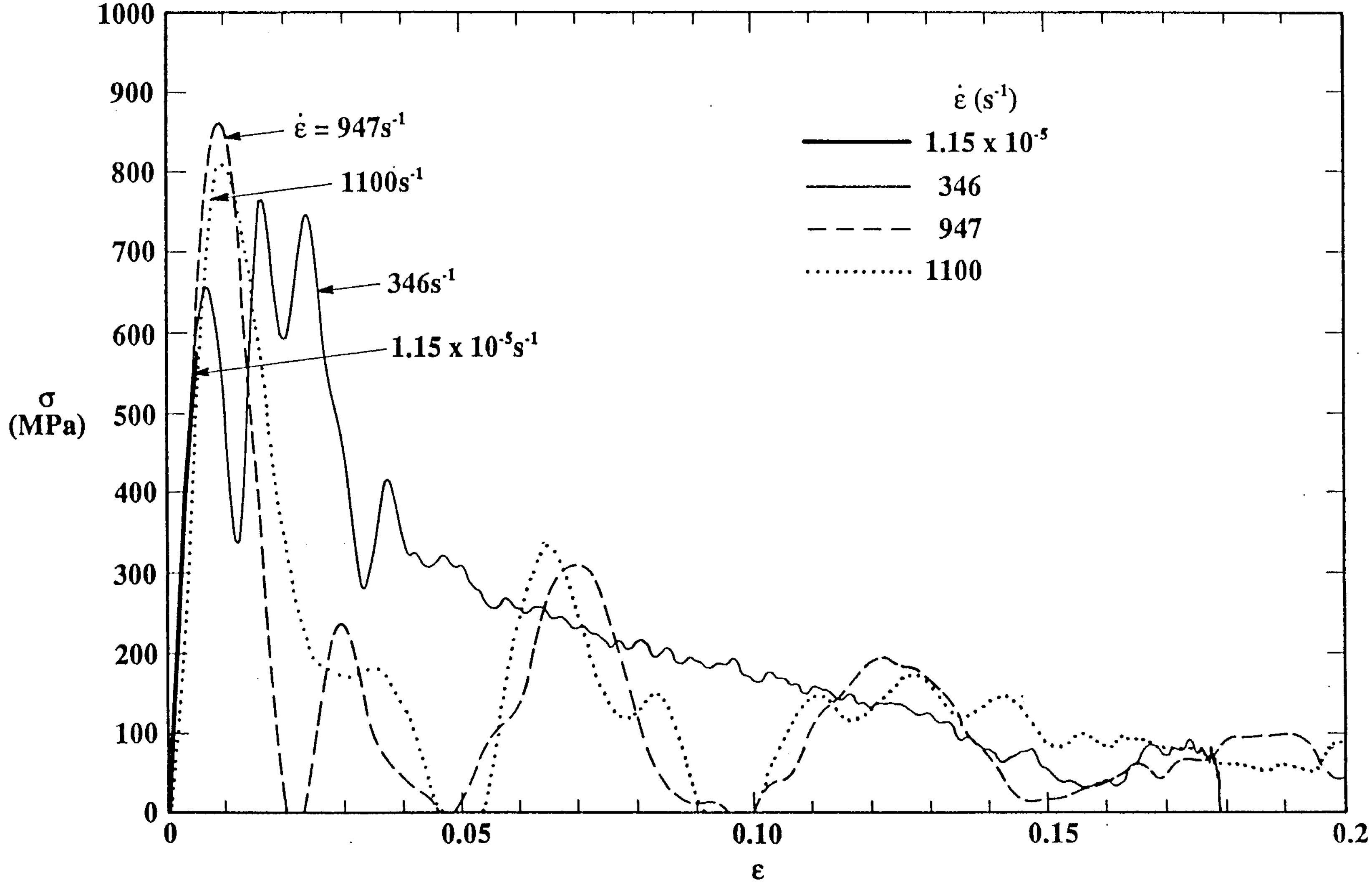

Figure 6. Quasi-static versus dynamic stress-strain response.

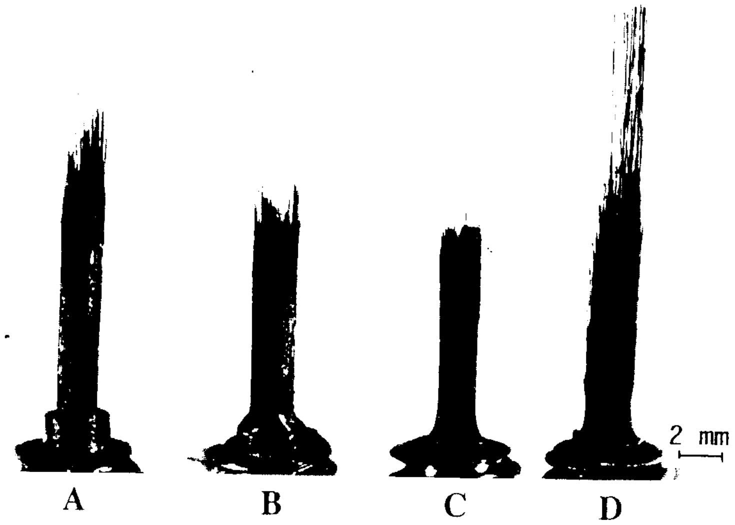

Figure 7. Macroscopic view of specimen failure, showing varying degrees of fiber pullout. (A) $\dot{\epsilon} = 1.15 \times 10^{-5}\ s^{-1}$; (B) $\dot{\epsilon} = 346 s^{-1}$; (C) $\dot{\epsilon} = 947 s^{-1}$; (D) $\dot{\epsilon} = 1100 s^{-1}$.

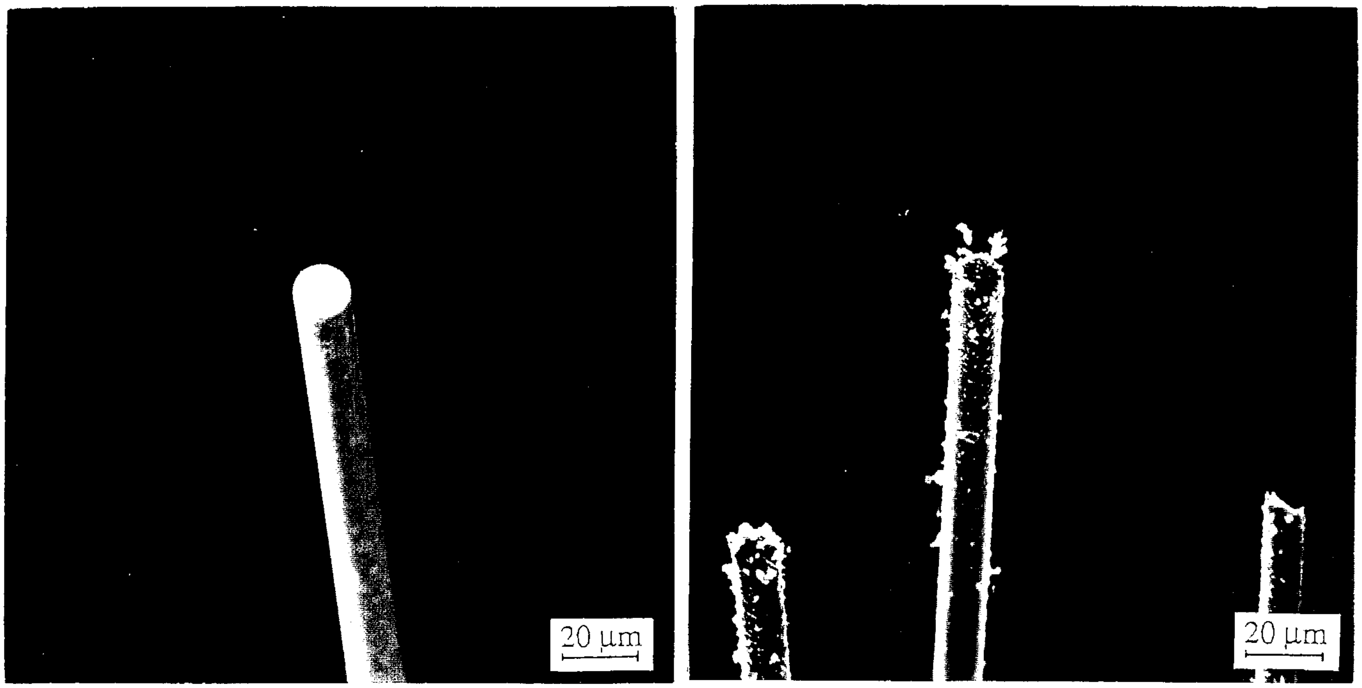

(A) $\dot{\varepsilon} = 1.15 \times 10^{-5}s^{-1}$; clean fibers. (B) $\dot{\varepsilon} = 947s^{-1}$; debris adhering to fibers.

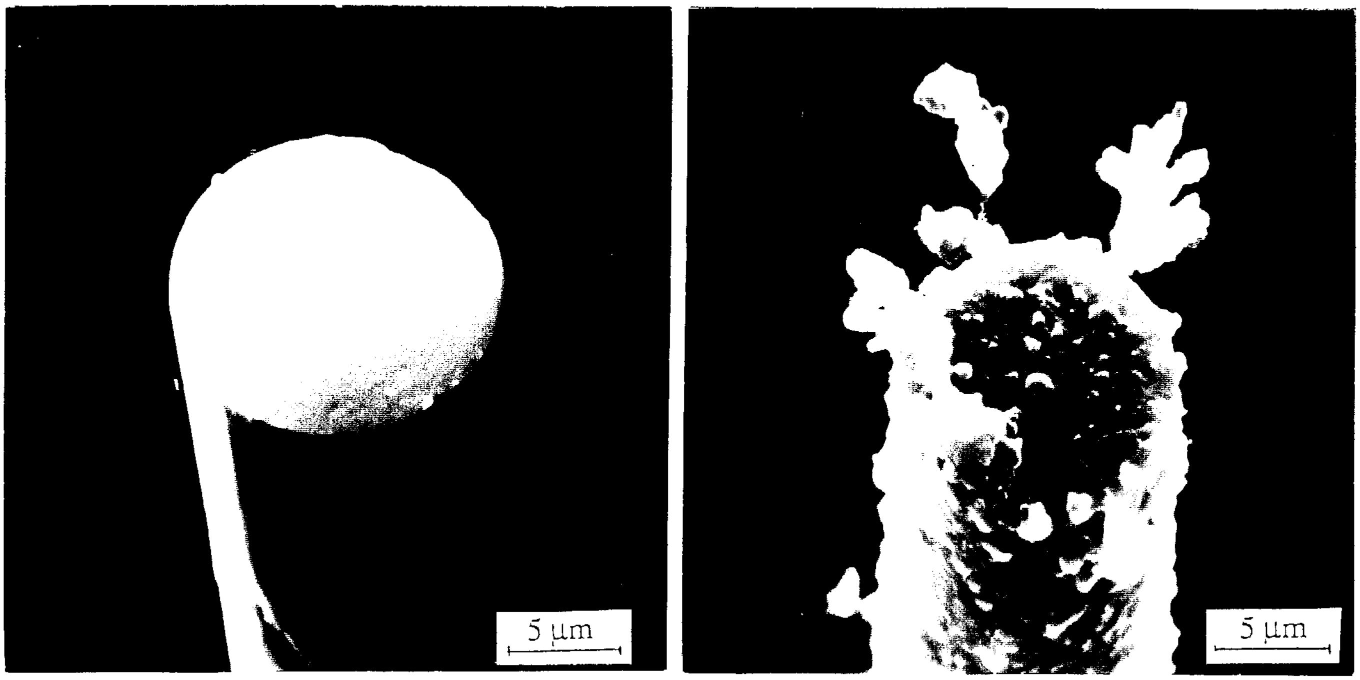

(C) Detail of (A). (D) Detail of (B).

Figure 8. SEM of pulled out fibers.

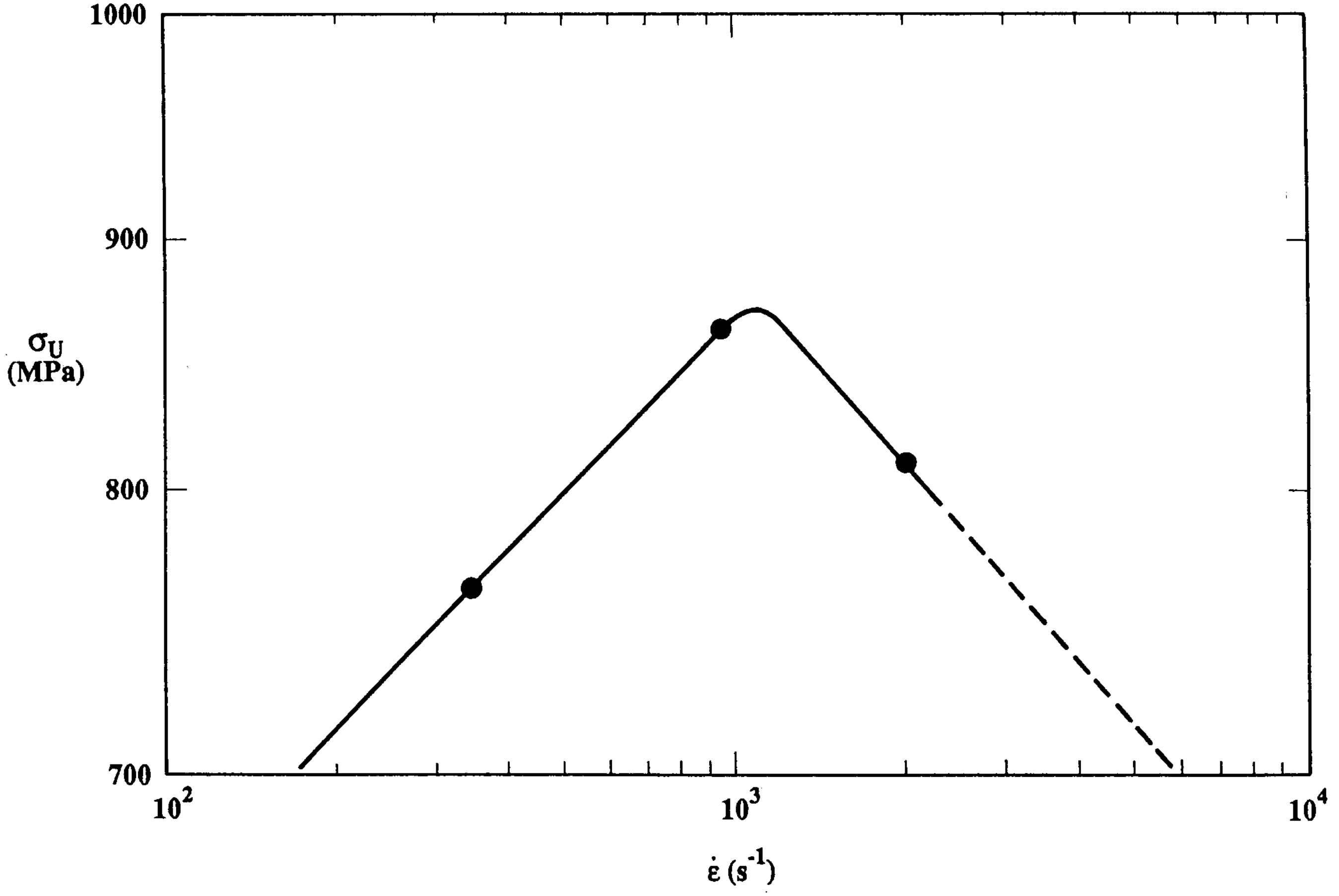

Figure 9. Ultimate strength versus dynamic strain rate.

# IV.

# Experimental Characterization of Kink Band Development in Polymeric Composites: A Report of Recent Progress

By
J. Lankford
Southwest Research Institute
San Antonio, Texas 78228-0510

## ABSTRACT

Means of capturing the critical events associated with compressive kink band nucleation and development have been investigated. Several promising approaches were developed, and the application of each to the problem is being pursued concurrently.

## BACKGROUND

During the last few years, the author has been investigating the compressive behavior of polymeric and ceramic matrix fiber reinforced composites under a variety of loading conditions, including wide ranges in strain rate[1-5] and confining pressure.[6-11] Based on these experiments, an example of which is shown in Figure 1, it has become clear that the compressive failure of polymeric composites is totally dominated by shear. This is reflected in the absolute independence of compressive strength differential upon confining pressure, which defines a critical shear stress $\left( \sim \frac{\sigma_1 - \sigma_3}{2} \right)$ for the strength of the composite.

It was found that in all cases the polymeric composite failed by kink band nucleation and growth. Independent work, principally by Lesko and his colleagues,[12-14] appears to indicate that both compressive strength and compressive fatigue life are affected by variation in interphase shear strength. Since kink band propagation under monotonically increasing load is a catastrophic process, it is most likely that the influence of the interphase manifests itself in the nucleation stage of kink development, as discussed elsewhere by the author.[15] Unfortunately, most current theories involving kink bands deal only with the growth process, which is fairly straight forward to model.[16-20] The micromechanics of kink band nucleation, however, are unknown and difficult to study, because the prekink site, being subsurface, usually is not available for characterization.

Accordingly, several approaches to the kink band nucleation problem were explored during the last year. Results, and plans for implementing the experimental techniques forthcoming, are outlined in the following section.

## Kink Band Nucleation Exploratory Research

A number of questions must be addressed in order to understand kink band nucleation. For example: Does fiber-matrix failure, pure matrix failure, or fiber fracture initiate a kink? How does the interphase manifest itself during kink-type failure, i.e., shear of interphase; alteration of stress (strain) transfer to adjacent fibers? What is the critical damage configuration that triggers kink nucleation?

As noted earlier, it appears virtually impossible to observe a kink actually nucleating within a three-dimension composite layup. Consequently, what is needed is a close look at the incremental development of existing kinks under stable subcritical conditions. In particular, the flexed, but not yet broken, fibers just ahead of the actual kink tip must behave like a nucleating kink, i.e., the subcritically propagating kink in essence is continually renucleating itself. Based on this postulate, a simple, pre-flawed (kinked) multi-fiber specimen is required. Because of the highly localized, small scale events associated with the kinking of a thin (10 μm) fiber, high magnification is necessary, together with the ability to characterize deformation and displacement (mode and amplitude) associated with interphase degradation and disbonding, and with local fiber fracture.

To generate prekinked compression specimens, we have followed the procedures shown in Figure 2. Notched unidirectional graphite fiber-reinforced PEEK has been loaded in four point flexure. With the notch on the compressive side, it is possible to nucleate a stable kink band. From the latter, a miniature compression sample can be machined, with only the smallest vestige of a kink precursor. An example of the result of this procedure is shown in Figure 3. In Figure 3(b), it is possible to discern microcracks in fibers in advance of the kink tip; these essentially define a kink "plastic zone," analogous to that attending a tensile crack tip. No matrix or fiber-matrix cracks are visible in this unloaded specimen.

In order to image and characterize the latter types of flaws, it is necessary to load the miniature specimens, as shown in Figure 4, and simultaneously observe the kink damage zone at high magnification. Experiments of this kind have begun in our laboratory, whereby the samples are being tested under monotonic and cyclic loading within the *in situ* SEM loading stage. Under these circumstances, matrix and interphase cracks open and become visible, and matrix deformation can be quantified using stereoimaging strain analysis.

Other experiments are aimed at characterizing the influence of the interphase on kink cyclic growth rate, as distinguished from kink initiation. This has proved to be somewhat tricky, since under conventional four point flexure, cracks readily nucleate, but swiftly transit to a splitting (nonkinking) mode of growth (Figure 5(a)). After considerable experimentation, it became clear that the splitting arose from the lack of restraint on the cross-fiber loading imposed by rotation of the compressive section of the sample at the lower loading points on the upward (tensile) portion of the load cycle. To defeat this anomalous mechanism, we have developed a modified 4-point flexure procedure, whereby the lower (compressive side) loading points are moved right to the edges of the notch (Figure 5(b)). With this arrangement, it is possible to nucleate cyclic loading. Typical data are shown in Figure 6, which essentially represent a single point on a da/dN versus $\Delta K_{kink}$ curve. The latter can be constructed by performing such experiments incrementally over a range in applied load to generate a corresponding range in $\Delta K_{kink}$.

Finally, experiments have been initiated involving the mesoindentation technique developed by Lesko, *et al.*[13] Acoustic emission and high resolution displacement measurements are being used to try to define the critical indenter displacement (hence critical fiber misalignment) required to nucleate a kink within a composite of a given interfacial shear strength.

## SUMMARY

The preceding set of protocols will be used in concert to address questions concerning the role of the interphase in compression failure. Samples of varying interphase strength are being prepared, and will be tested and evaluated during the next phase of the program.

## REFERENCES

1. Lankford, J., "Strength of Monolithic and Fiber-Reinforced Glass Ceramics at High Rates of Loading and Elevated Temperature," *Ceramic Engineering and Science Proceedings*, **9**, 843 (1988).

2. Lankford, J., "Dynamic Compressive Fracture in Fiber-Reinforced Ceramic Matrix Composites," *Material Science and Engineering*, **A107**, 261-268 (1989).

3. Lankford, J., "Compressive Damage and Failure at High Loading Rates in Graphite Fiber-Reinforced Polymeric Matrix Composites," *Ceramic Transactions*, **19**, Advanced Composite Materials, edited by M. D. Sacks, The American Ceramic Society, Westerville, OH, pp. 553 (1991).

4. Lankford, J., Couque, H., and Nicholls, A., "Effect of Dynamic Loading on Tensile Strength and Failure Mechanisms in a SiC Fiber-Reinforced Ceramic Matrix Composite," *Journal of Materials Science*, **27**, 920-936 (1992).

5. Lankford, J., "Micromechanisms of Compressive Failure in a Glass Fiber-Reinforced Amorphous Thermoplastic," *Journal of Materials Science*, **28**, 3027-3034 (1993).

6. Lankford, J., "The Compressive Failure of Polymeric Composites Under Hydrostatic Confinement," *Composites* (in press).

7. Couque, H., Albertini, C., and Lankford, J., "Failure Mechanisms in a Unidirectional Fiber-Reinforced Thermoplastic Composite Under Uniaxial, In-Plane Biaxial, and Hydrostatically Confined Compression," *Journal of Materials Science Letters*, **12**, 1953-1957.

8 Lankford, J., "The Effect of Hydrostatic Pressure and Loading Rate on Compressive Failure of Fiber-Reinforced Ceramic Matrix Composites," *Composite Science and Technology*, **51**, 537-543 (1994).

9. Lankford, J., "Dynamic Compressive Failure of Brittle Materials Under Hydrostatic Confinement," *Experimental Techniques in the Dynamics of Deformable Solids*, AMD-Vol. 165, edited by K. T. Ramesh, ASME, NY, pp. 1-10 (1993).

10. Lankford, J., "Utilization of the Split Hopkinson Pressure Bar Under Hydrostatic Confining Pressure to Characterize the Compressive Behavior of Ceramics and Ceramic Composites," *Mechanical Testing of Ceramics and Ceramic Composites*, edited by A. Gilat, TMS AIME, NY, pp. 1-11 (1994).

11. Lankford, J., "Shear Versus Dilatational Damage Mechanisms in the Compressive Failure of Fiber-Reinforced Composites," *Composites* (in press).

12. Lesko, J. J., Swain, R. E., Cartwright, J. M., Chin, J. W., Reifsnider, K. L., Dillard, D. A., and Wightman, J. P., *J. Adhesion* (in press).

13. Lesko, J. J., Elmore, J. S., Case, S. W., Swain, R. E., Reifsnider, K. L., and Dillard, D. A., ASTM STP, American Society for Testing and Materials, Philadelphia, PA (in press).

14. Lesko, J. J., ONR Workshop, Washington, DC, December, 7, 1994.

15. Lankford, J., "Compressive Failure of Fiber-Reinforced Composites: Buckling, Kinking, and the Role of the Interphase," *Journal of Materials Science* (in press).

16. Budiansky, B., and Fleck, N. A., "Compressive Failure of Fibre Composites," *J. Mech. Phys. Solids*, **41**, 183-211 (1993).

17. Slaughter, W. S., and Fleck, N. A., "Compressive Fatigue of Fibre Composites," *J. Mech. Phys. Solids*, **41**, 1265-1284 (1993).

18. Soutis, C., Fleck, N. A., and Smith, P. A., "Compression Fatigue Behavior of Notched Carbon Fibre-Epoxy Laminates," *Int. J. Fatigue*, **13**, 303-312 (1991).

19. Soutis, C., and Fleck, N. A., "Static Compression Failure of Carbon Fibre T800/924C Composite Plate With a Single Hole," *J. Comp. Mater.*, **24**, 536-558 (1990).

20. Sutcliffe, M.P.F., and Fleck, N. A., "Microbuckle Propagation in Carbon Fibre-Epoxy Composites," *Acta Metall. Mater.*, **42**, 2219-2231 (1994).

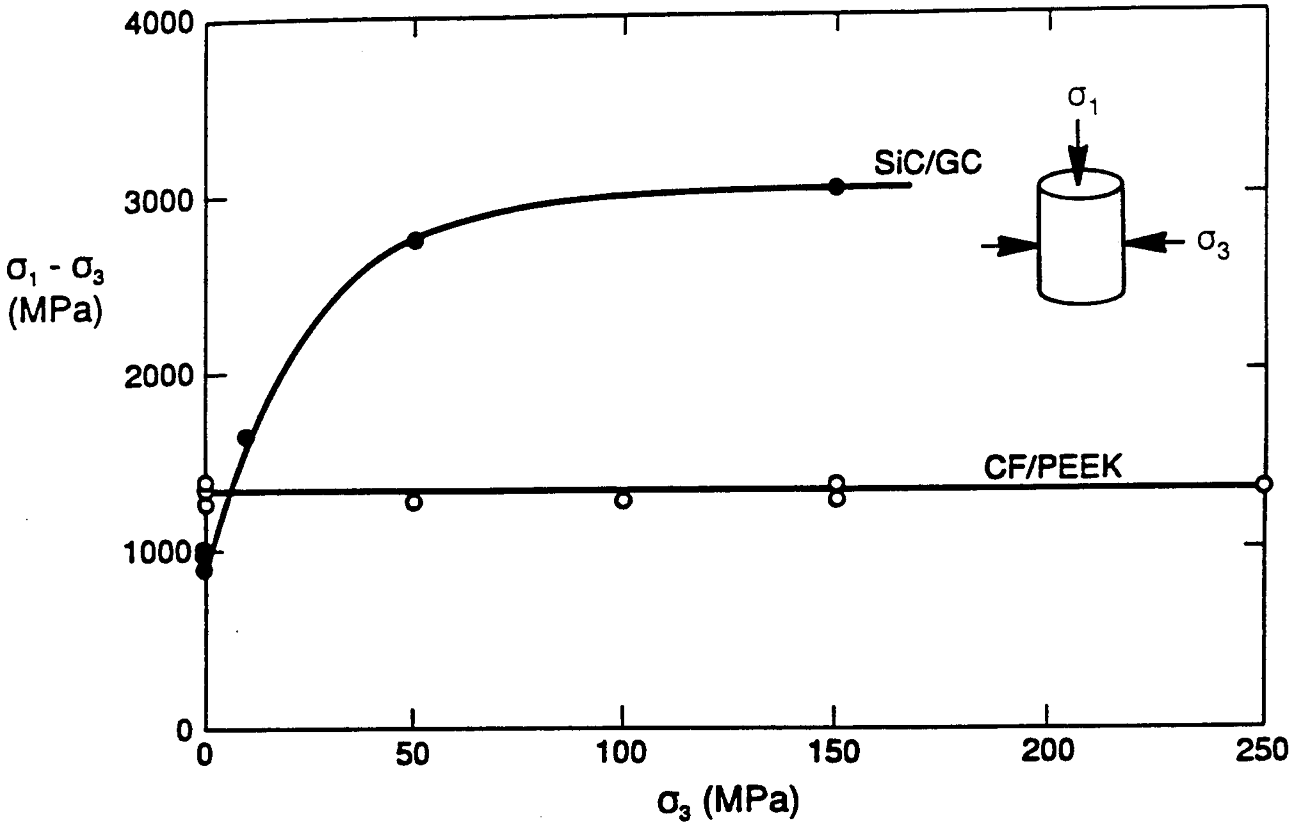

Figure 1. Compressive strength versus confining pressure for 0° carbon fiber-reinforced PEEK SiC fiber-reinforced glass ceramic.

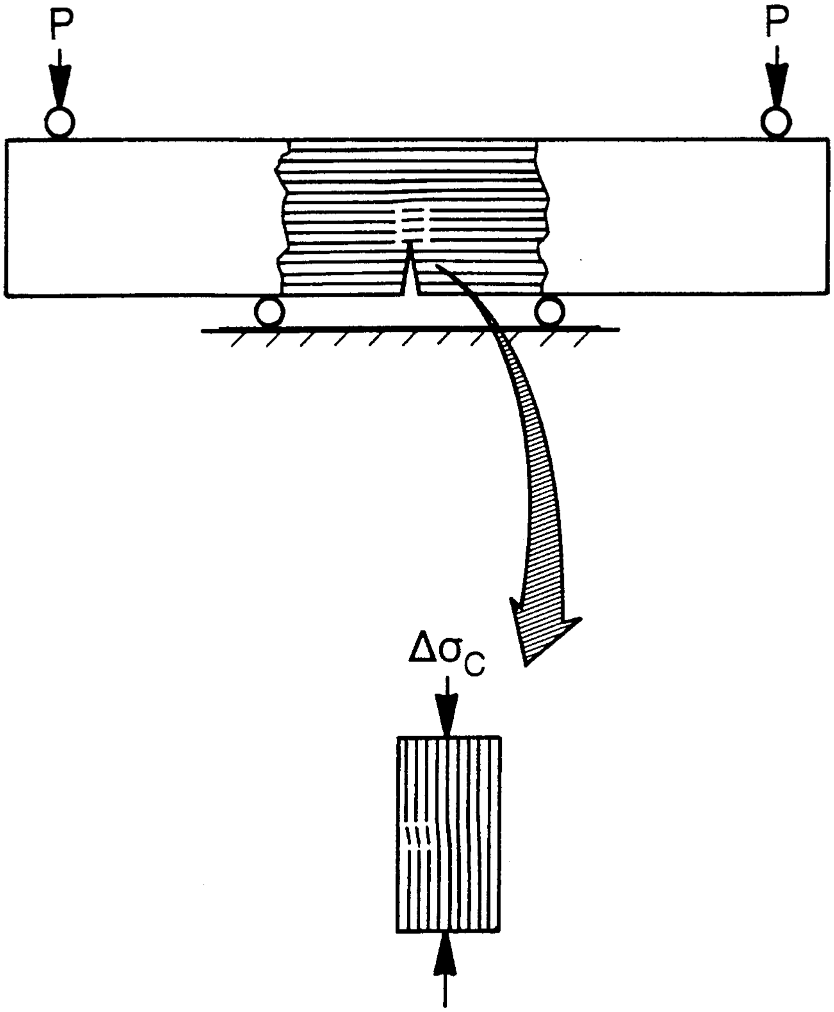

Figure 2. Procedure for obtaining prekinked cyclic compression specimen from edge-notched flexural sample used to generate kink.

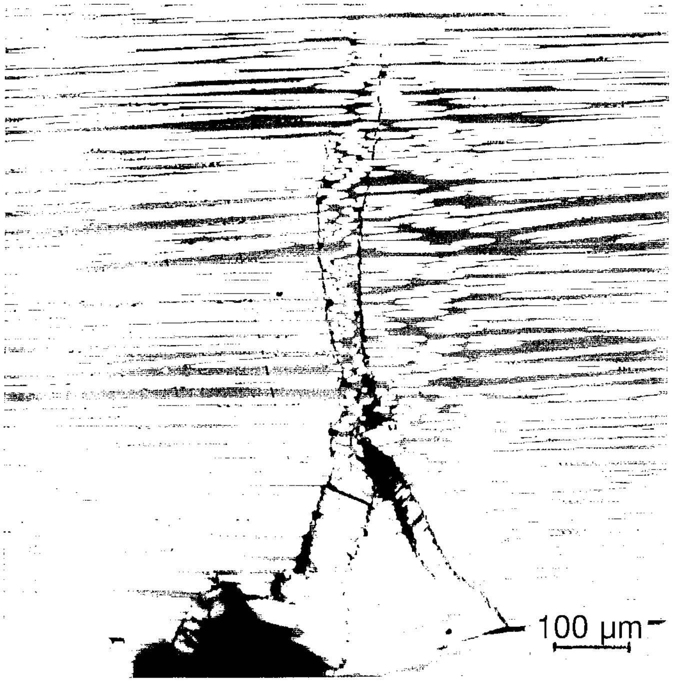

(a) Macroscopic kink band in notched flexural specimen.

(b) Microscopic kink band in miniature compression sample obtained from notched flexural specimen.

Figure 3. Typical kink band in flexural (parent) and miniature compression (daughter) specimens.

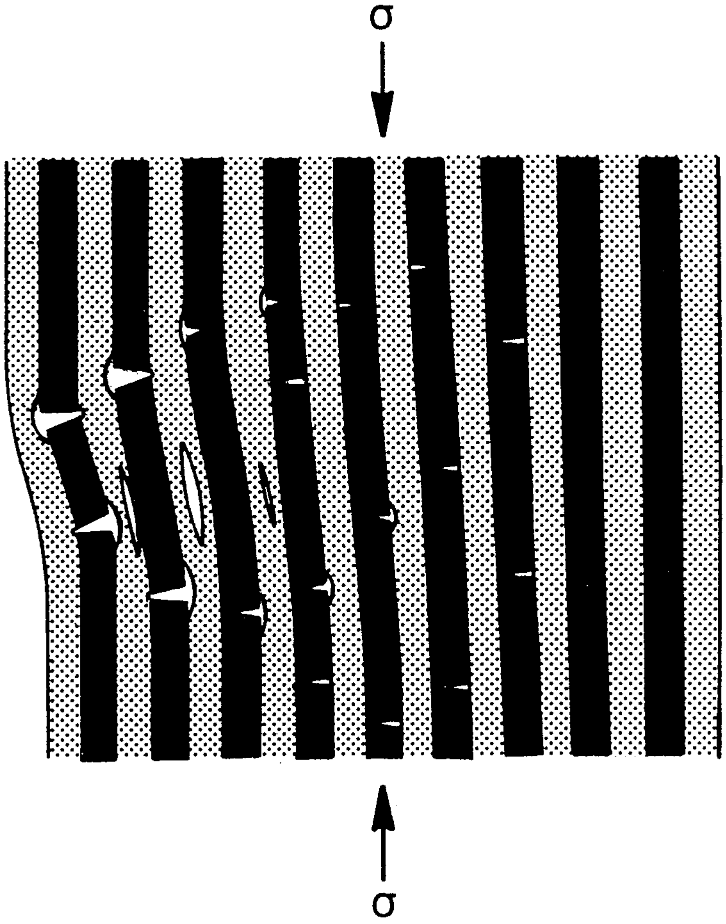

Figure 4. Kink band damage development under compressive load.

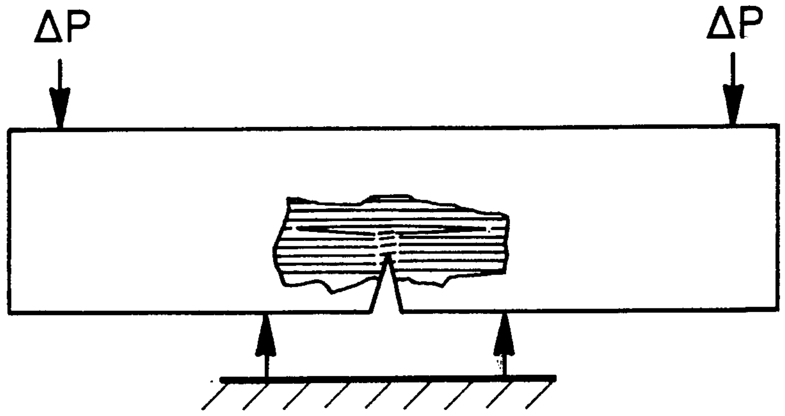

(a) Conventional 4-point flexure: transition from cyclic kinking to splitting.

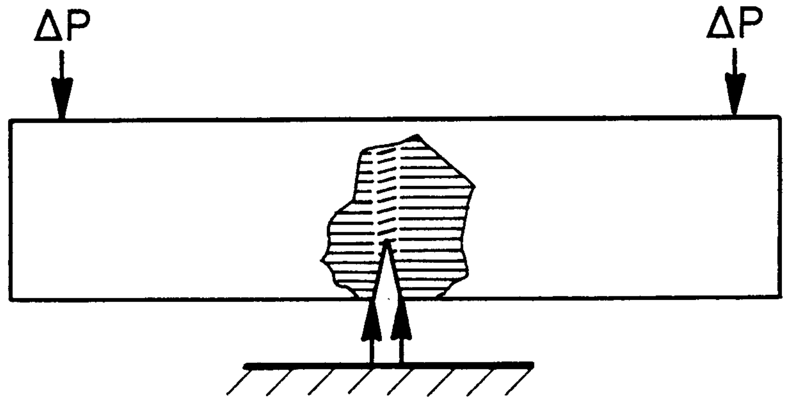

(b) Modified 4-point flexure: stable cyclic kink growth.

Figure 5. Procedure used to generate stable growth of compressive kink bands in 0° layup under cyclic loading.

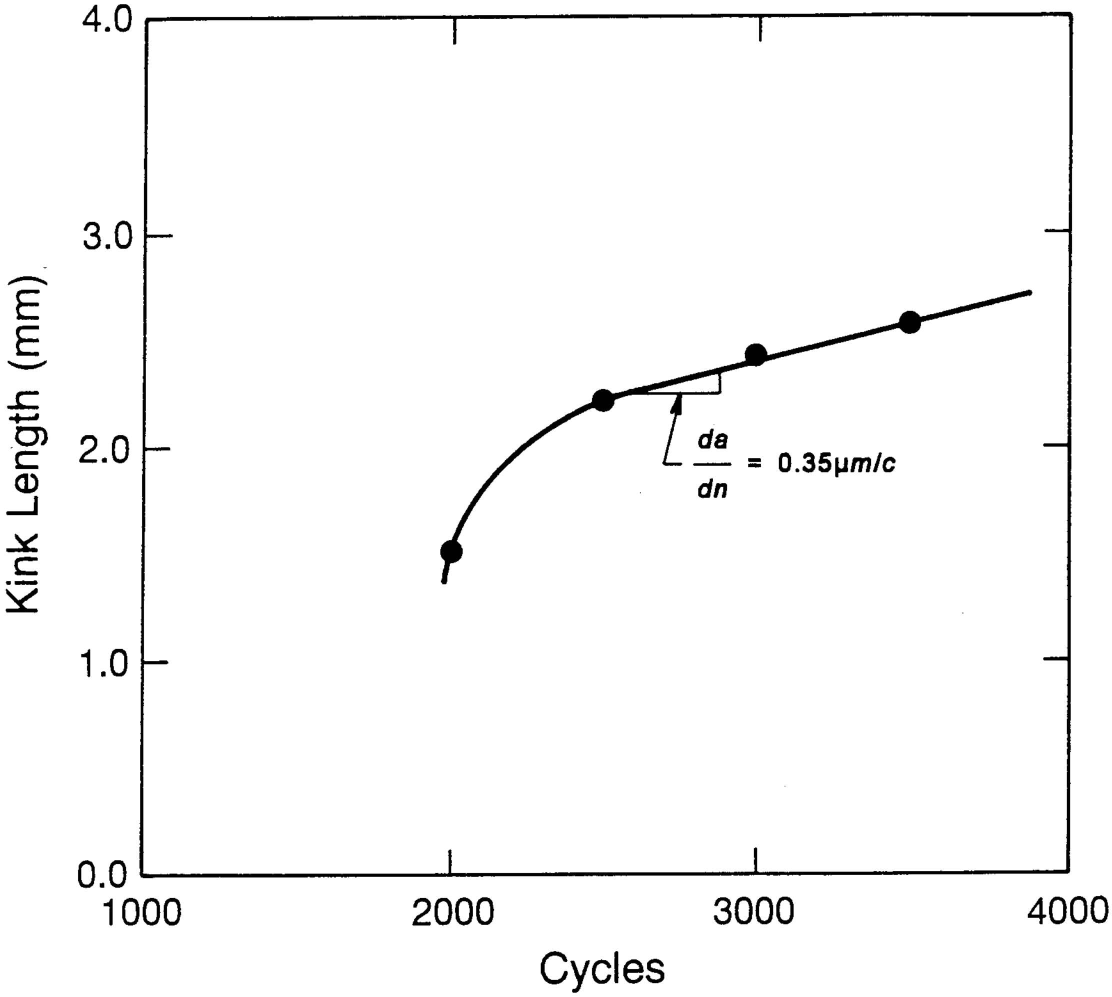

Figure 6. Stable growth of a compressive kink band in modified 4-point flexure, under a constant cyclic load.